

Master's Thesis

Xueting Wang 2015

LAPPEENRANTA UNIVERSITY OF TECHNOLOGY  
Faculty of Technology  
Chemical and Process Engineering

Xueting Wang

**AN EDTA- $\beta$ -CYCLODEXTRIN ADSORBENT FOR THE ADSORPTION OF RARE  
EARTH ELEMENTS AND ITS APPLICATION IN PRECONCENTRATION OF  
ULTRATRACE RARE EARTH ELEMENTS FROM SEAWATER**

Examiner: Prof. Mika Sillanpää

Instructors: D.Sc. (tech) Eveliina Repo

M.Sc. Feiping Zhao

## **ABSTRACT**

Lappeenranta University of Technology  
Faculty of Technology  
Chemical and Process Engineering

Xueting Wang

### **An EDTA- $\beta$ -cyclodextrin adsorbent for the adsorption of rare earth elements and its application in preconcentration of ultratrace rare earth elements from seawater**

Master Thesis

2015

77 pages, 13 figures, 15 tables

Examiner: Prof. Mika Sillanpää

Keywords: adsorption, REEs (rare earth elements), EDTA- $\beta$ -CD (ethylene diamine tetraacetic acid-cross-linked- $\beta$ -cyclodextrin), preconcentration, capacity

The objectives of this work were synthesizing an EDTA- $\beta$ -CD adsorbent and investigating its adsorption potential and applications in preconcentration of REEs from aqueous phase. The adsorption capacity of EDTA- $\beta$ -CD was investigated. The adsorption studies were performed by batch techniques both in one- and multi-component systems. The effects of pH, contact time and initial concentration were evaluated. The analytical detection methods and characterization methods were presented.

EDTA- $\beta$ -CD adsorbent was synthesized successfully with high EDTA coverage. The maximum REEs uptake was 0.310 mmol g<sup>-1</sup> for La(III), 0.337 mmol g<sup>-1</sup> for Ce(III) and 0.353 mmol g<sup>-1</sup> for Eu(III), respectively. The kinetics of REEs onto EDTA- $\beta$ -CD fitted well to pseudo-second-order model and the adsorption rate was affected by intra-particle diffusion. The experimental data of one component studies fitted to Langmuir isotherm model indicating the homogeneous surface of the adsorbent. The extended Sips model was applicable for the isotherm studies in three-component system. The electrostatic interaction, chelation and complexation were all involved in the adsorption mechanism. The preconcentration of RE ions and regeneration of EDTA- $\beta$ -CD were successful. Overall, EDTA- $\beta$ -CD is an effective adsorbent in adsorption and preconcentration of REEs.

## **ACKNOWLEDGEMENTS**

This Master Thesis was performed in Laboratory of Green Chemistry in Mikkeli from October 2014 to April 2015. I would like to thank examiner Mika Sillanpää, head of LGC and PhD student Feiping Zhao for their endless help in my thesis work. I would like to thank Eveliina Repo for her instructions in equipment and thesis revision. I also want to thank rests of researchers in Laboratory of Green Chemistry for their help and instructions during this period.

I am sincerely grateful to all the colleagues, professors and friends I have met during my Master's study in Lappeenranta University of Technology. They have given me knowledge, experience and happiness. I also want to thank my family for their support and understanding.

Mikkeli 15.04.2015

Xueting Wang

## TABLE OF CONTENTS

<b>Symbols and abbreviations</b> .....	<b>6</b>
<b>1 Introduction</b> .....	<b>10</b>
1.1 Objectives and contents .....	11
<b>2 Rare earth elements</b> .....	<b>12</b>
2.1 Applications and prospects of REEs.....	13
<b>3 Adsorption</b> .....	<b>15</b>
3.1 Adsorption kinetics .....	15
3.1.1 Pseudo-first-order .....	16
3.1.2 Pseudo-second-order .....	17
3.1.3 Intra-particle diffusion.....	17
3.2 Adsorption isotherm models .....	18
3.2.1 Langmuir isotherm model .....	18
3.2.2 Freundlich isotherm model.....	19
3.2.3 Dubinin-Radushkevich (D-R) isotherm model.....	20
3.2.4 Sips (Langmuir-Freundlich) isotherm model .....	21
3.2.5 BiLangmuir isotherm model.....	23
3.2.6 BET (Brunauer, Emmet, Teller) isotherm model.....	23
3.2.7 Isotherm models for multi-components system.....	24
3.2.8 Extended Sips isotherm model .....	25
3.2.9 Extended BiLangmuir isotherm model.....	26
3.3 Adsorption capacity and desorption ratio .....	27
<b>4 Analytical methods for determining REEs in liquid phase and characterization methods for adsorbents</b> .....	<b>29</b>
4.1 Inductively Coupled Plasma-Optical Emission Spectrometry (ICP-OES) .....	29
4.2 Inductively Coupled Plasma-Mass Spectrometry (ICP-MS) .....	30
4.3 Characterization methods used for adsorbents.....	32
4.4 Other used methods .....	32
<b>5 Adsorbents used in adsorption of REEs</b> .....	<b>33</b>
5.1 Adsorbents used in this research.....	33
<b>6 Experimental testing</b> .....	<b>36</b>
6.1 ICP .....	36
6.2 Preparation of adsorbents.....	37
6.3 Preparation of samples.....	38
6.3.1 Samples preparation for pH studies.....	39
6.3.2 Samples preparation for contact time studies .....	39
6.3.3 Samples preparation for different initial concentrations.....	40

6.3.4	Samples preparation for Multi-component REE systems studies.....	41
6.3.5	Samples preparation for preconcentration of REEs studies from pure water, tap water and seawater	42
6.4	Batch adsorption .....	42
6.4.1	Adsorption in mono-component system.....	43
6.4.2	Adsorption in Multi-component REE systems .....	44
6.4.3	Preconcentration of REEs studies from pure water, tap water and seawater.....	44
6.5	Preparation standard solutions for ICP .....	45
<b>7</b>	<b>Results for experimental testing .....</b>	<b>46</b>
7.1	Characterizations of EDTA- $\beta$ -CD and EPI- $\beta$ -CD.....	46
7.2	Effects of pH.....	49
7.3	Effect of contact time and adsorption kinetics.....	50
7.4	Adsorption isotherm .....	53
7.5	Adsorption in multi-component systems .....	57
7.6	Adsorption mechanism .....	60
7.7	Preconcentration of REEs studies from pure water, tap water and seawater .....	63
<b>8</b>	<b>Conclusion .....</b>	<b>64</b>
<b>9</b>	<b>Summary.....</b>	<b>66</b>
	<b>References.....</b>	<b>69</b>

**Symbols and abbreviations**

AA	acrylic acid
APT	attapulgate
$\beta$ -CD	$\beta$ -cyclodextrin
CD	cyclodextrin
CDP	CD polymers
$\text{CHCl}_3$	chloroform
COD	chemical oxygen demand
D151	macroporous weak acid resin
DMF	dimethyl formamide
DTPA	diethylene triamine pentaacetic acid
EDS	energy dispersive X-ray spectrometer
EDTA	ethylene diamine tetraacetic acid
EDTA- $\beta$ -CD	EDTA-cross-linked $\beta$ -cyclodextrin
EGTA	ethylene glycol tetraacetic acid
EPI	epichlorohydrin
EPI- $\beta$ -CD	EPI-cross-linked $\beta$ -cyclodextrin
FTIR	Fourier transform infrared spectroscopy
GMZ	Gao Miao Zi
GFAAS	Graphite Furnace Atomic Absorption Spectroscopy

HESI-SBA-15 a ligand of SBA-15 with covalently bonded N-(2-hydroxyethyl) salicylaldehyde Schiff base

HNO<sub>3</sub> nitric acid

HPC hydroxypropyl cellulose

HPC-g- PAA/APT grafting reaction of acrylic acid onto hydroxypropyl cellulose with attapulgate

H,PEG400,PMo/PW a crystalline sorbent prepared by the reaction of PEG with PMo and PW heteropolyacids

HREEs heavy rare earth elements

HyLBA hybrid Lewis base adsorbent

ICP inductively coupled plasma

ICP-OE inductively coupled plasma optical emission

ICP-OES inductively coupled plasma optical emission spectrometry

ICP-MS inductively coupled plasma-mass spectrometry

LDH-A layered double hydroxide (A<sup>-</sup> anion of carrier)

LREEs light rare earth elements

M mol/L

MgFe-LDH-A MgFe layered double hydroxides (A<sup>-</sup> anion of carrier)

M-PAM magnetic polyacrylamide

M-PAM-HA magnetic hydroxamic acid modified polyacrylamide

MREEs medium rare earth elements

MSP	sodium dihydrogen phosphate
NCs	nanocomposites
PEG-200	polyethylene glycol 200
PMo	phosphomolybdic
PW	phosphotungstic
RE	rare earth
REEs	rare earth elements
REO	rare earth oxides
SBA-15	mesoporous molecular sieve
SEM	scanning electron microscope
STP	standard temperature and pressure
TGA	thermogravimetric analysis
TREO	total rare earth oxides
Ce	cerium
Dy	dysprosium
Er	erbium
Eu	europium
Gd	gadolinium
Ho	holmium
La	lanthanum

Lu	lutetium
Nd	neodymium
Pm	promethium
Pr	praseodymium
Sc	scandium
Sm	samarium
Tb	terbium
Tm	thulium
Y	yttrium
Yb	ytterbium
Ce <sup>3+</sup>	cerium cation
Eu <sup>3+</sup>	europium cation
La <sup>3+</sup>	lanthanum cation
Nd <sup>3+</sup>	neodymium cation

## 1 Introduction

REEs have been widely applied in mundane (lighter flints, fluorescent lamps), high-tech (batteries, lasers, magnets, phosphors), and futuristic (high-temperature superconductivity, storage, conservation and transport of energy) fields according to their diverse nuclear, chemical, electrical, metallurgical, magnetic, optical, and catalytic properties (Gordon *et al.* 2002, 087-02). However, REEs are typically dispersed and it is difficult to be concentrated as rare earth minerals in exploitable ore deposits compared to ordinary base and precious metals (Keith Veronese). Consequently, the mineable REEs are very scarce as the name indicates. Recently, with ever-increasing REEs demand, the recovery and separation of REEs from aqueous streams such as industrial wastewater or seawater is crucial because this way could supplement the demand of REEs from mining industry (Lou *et al.* 2015, 1333–1341).

Several traditional separation methods have been used to separate or preconcentrate REEs since the first REE was found, such as co-precipitation, crystallization, solvent extraction, and ion-exchange. However, they have disadvantages such as secondary pollution, inefficiency, high-cost, unstable and low regeneration possibility and selectivity. Therefore, finding a better way is increasingly demanded. For the last few decades, adsorption has drawn more and more researchers' attention to be a very attractive and promising method to concentrate or separate metal ions due to its non-toxicity, reusability, ease of operation, and the abundance of adsorbents in nature. (Zhu *et al.* 2015, 410)

Various adsorbents for recovery and preconcentration of REEs have been investigated, such as activated carbon (Murty *et al.* 1996, 815-820), chitosan (Zhao *et al.* 2015, 1271-1281), cellulose (Zhu *et al.* 2015, 410),  $\beta$ -cyclodextrin (Han *et al.* 2009), silica (Esser *et al.* 1994, 1736–1742), titanium dioxide (Liang *et al.* 2001, 863-866) and aminocarboxylic sorbents (Grebneva *et al.* 1996, 1417–1423).

Recently, we prepared an EDTA- $\beta$ -CD adsorbent by a simple and green approach via the

polycondensation reaction of  $\beta$ -CD with EDTA. The adsorption behaviors and preconcentration applications of REEs onto EDTA- $\beta$ -CD were investigated in this work.

### **1.1 Objectives and contents**

In this work, EDTA- $\beta$ -CD was used to adsorb La(III), Ce(III), and Eu(III) from aqueous solutions. The effects of variables including pH, contact time, REE initial concentration on the adsorption capacity, selectivity and regeneration properties of the EDTA- $\beta$ -CD were investigated. To understand the adsorption mechanism, the experimental data was further fitted to kinetic and isotherm models. Additionally some characterization methods like Fourier transform infrared spectroscopy (FTIR) and elemental distribution mapping were also employed to verify the mechanism. Furthermore, to assess its practicability in real case, the as-prepared adsorbent was used for separation and preconcentration of REEs from different water matrices.

In the theory part, the properties of REEs will be introduced shortly. Then, the relevant adsorption kinetics and isotherm models were described. The mainly used analytical and characterization method were presented briefly. Moreover, the adsorbents used in this work were introduced shortly. In the experimental part, the synthesis method of adsorbents and all the materials and experiments procedures were depicted detailed. After the experimental part, all the results will be illustrated and discussed. The final conclusions and the whole thesis were summarized.

The experiments was completed in Laboratory of Green Chemistry in Mikkeli. During the seven months period, large amount of articles were read concerning adsorption of REEs from wastewater and many experiments were done. Based on this work, one relevant article might be published afterwards.

## 2 Rare earth elements

REEs are composed of all lanthanides and the other two elements Sc and Y in the periodic table of elements according to the International Union for Pure and Applied Chemistry (IUPAC). REEs have similar atomic structure, chemical and physical properties (Christmann, 2014, 19). Besides, according to their good magnetic, optical, electrical, chemical and catalytic properties, REEs are applied into many industrial and analytical applications, such as petrochemical industry, hydrometallurgy, electronic industry, energy, agricultural and so on (Zhu *et al.* 2015, 410).

REEs are “rare” because they are rare in metallic forms, only as mixtures and difficult to separate. Actually they are abundant in Earth’s crust except radioactive promethium, for instance, Ce is the most abundant REEs comprising Earth’s crust, even more than copper and lead. They are found mostly in their dispersion phases. Therefore, it is not easy to find pure and enriched REEs in their natural state.

Normally REEs can be divided into two groups LREEs and HREEs according to their differences in solubility which are shown in Table 1 (Christmann, 2014, 19-20).

**Table 1.** The category of REEs.

<b>LREEs</b>	La	Ce	Pr	Nd	Pm	Sm						
<b>HREEs</b>	Eu	Gd	Tb	Dy	Ho	Er	Tm	Yb	Lu	Y	Sc	

All the REEs have similarities in atomic structure, ionic radius, chemical and physical properties, and they can coexist in natural sources. They are all very active metals. Most REEs are paramagnetic. The most common valence is trivalent. Their hydrated ions are colored. It is very easy for REEs to form stable coordination compounds. Most REEs metals are malleable and ductile. It is very easy for them to be oxidized rapidly and the most common state is their oxidation state (REO). They react with all halogens and can dissolve readily in dilute sulfuric acid.

## 2.1 Applications and prospects of REEs

REEs just entered into commercial markets 50 years ago (Stephen *et al.*). LREEs occupy 66.8% of global demand in 2012 (Ponou *et al.* 2014, 1070). The production of REE products is dominated by China, United States and Australia; however, according to the reserve of REEs, China is estimated to occupy over 90% of the world total reserve (Moldoveanu *et al.* 2012, 71).

Among all the REEs, promethium is unstable and radioactive with a total naturally available quantity in the Earth's crust of 21 grams. Hence, it has no economic significance. The conventional deposits of REEs are related to carbonatites and hyperalkaline intrusives. However, sedimentary phosphate deposit may be one potential future source of REEs which will be a very important supply to the world economy. (Christmann, 2014, 24)

REEs are mainly applied in high-tech industries. Actually, there are more than 400 ongoing rare earth exploration projects all over the world according to the research of Christmann (2014, 19-26). Particularly some elements are really rare, such as dysprosium, europium and terbium which are in high demanding, since they are indispensable to the production of Fe-B-Nd (Dy) permanent magnets, which is currently the only available material in industrial scale. Moreover, they are also essential in the production of phosphors, which can be used in light bulbs or fluorescent.

As mentioned above, all REE elements exist jointly in each deposit. This can be regarded as a potential REEs markets. In fact, each production of one particular HREE element, such as europium, dysprosium and terbium, will bring about large quantities of LREEs production, such as lanthanum and cerium. This is the coupling of REE production. For instance, the production of 1 ton of dysprosium will bring about coupling production of 20 tons of lanthanum and 35 tons of cerium. (Christmann, 2014, 21)

Table 2 shows a detailed overview of different REEs applications. This table provides data on the quantities of total rare earth oxides (TREO) requirement of 2011 in the main

applications as well as the tentative estimation of TERO requirements of 2020 in these usages. According to Christmann, this table is derived from a presentation by Dudley Kingsnorth to the German (public) Raw Material Agency (Deutsche Rohstoffagentur) (Christmann, 2014, 21).

**Table 2.** 2011 TERO consumption by the main market segments and scenarios for 200 consumption, based on current Compound Average Growth Rates-Derived from D.Kingsnorth (Christmann, 2014, 21).

			2011 Production [Metric tons]	2020 demand scenario of rare earth
Permanent Magnets	Nd,Dy,Pr	Windmills, hard-disk drives, automobile, defense and many more	21000	42000-69900
NiMh batteries	La,Ce	Batteries, especially in hybrid vehicles	21000	3000-50300
Phosphors	Eu,Tb,Y,Ce, Dy,Gd,La,Pr	Video screens (TV, computers);compact fluorescent light bulbs, LEDs, banknotes	8000	12000-20000
Catalysts for the oil & gas industry	La,Ce,Pr,Nd	Cracking of larger hydrocarbon molecules into light products for the production of fuels	20000	22300-37100
Polishing powder	Ce,La,Nd	Polishing powder for automobile windshields	14000	16300-27100
Catalysts for the automotive industry	Ce,La,Nd	Reduction of particulates, SOX and NOX in exhaust gas	7000	10100-16800
Glass industry	Ce,La,Nd,Er ,Pr,Eu	UV filtering (Ce in windshields),La for optical glass (cameras), other for coloring	8000	8900-14900

### 3 Adsorption

Normally there are two kinds of adsorption, chemical adsorption (chemisorption) and physical adsorption (physisorption) according to the nature of forces existing between adsorbent and adsorbate. In physisorption, the attraction force between the adsorbent and adsorbate is Vander Waal's force, which is very weak and makes desorption easy. Whereas, in chemisorption, the attraction forces between adsorbent and adsorbate is the same strength as chemical bond, which is relatively strong and can make desorption difficult. (Heinonen 2012, 17)

There are many variables affecting adsorption behaviors, mainly pH, contact time, initial concentration. Based on the previous research by Zhang *et al.* (2009, 112), the experiments are carried out in temperature range from 0°C to 50°C with no effect on the adsorption amounts (>98%) of La<sup>3+</sup> by H,PEG400,PW and H,PEG400,PMo. Therefore, the temperature is not a significant factor affecting adsorption process. Hence, most of the previous research were performed at room temperature.

#### 3.1 Adsorption kinetics

Adsorption kinetics depict the adsorbates uptake rate as function of contact time between solid and liquid phase including intra-particle diffusion process. (Ponou *et al.* 2014, 1075)

The optimal contact time depends on process, adsorbents and adsorbates conditions. Therefore, it varies from minutes to hours. The adsorbents can be porous or imporous. Some studies have shown that the adsorption rate is faster in imporous adsorbents compared to porous adsorbents. The reason might be that the adsorption sites in some imporous adsorbents are more accessible for cations. (Ngomsik *et al.* 2012, 7)

Normally, the adsorption process consists of two stages. In the first stage, the rate of adsorption is always very fast because of abundant of adsorption sites available. Then in the second stage, the rate of adsorption will goes down because of saturation of the

adsorbents. Metal ions will form aggregations around the sites. Based on that, the adsorption capacity can scarcely be increased when contact time is extended. (Zhu *et al.* 2015, 413)

It is well known that adsorption could be determined by various mechanisms such as mass transfer, chemical reaction, and particle diffusion (Hokkanen *et al.* 2013, 40-47). Adsorption kinetic studies are very helpful to understand adsorption mechanism of metals and can be used as an indicator to estimate the adsorption efficiency of adsorbent. The adsorption kinetics can be evaluated based on pseudo-first-order equation and pseudo-second-order equation (Zhu *et al.* 2015, 414). To determine the rate-determining step and the effect of contact time during adsorption process, pseudo-first-order and pseudo-second-order should be employed based on the experiment data (Zhao *et al.* 2014, 51). Sometimes intra-particle diffusion should also be taken into account.

### 3.1.1 Pseudo-first-order

Pseudo-first-order assumes that the rate of change in adsorbed adsorbate amount with time is directly proportional to difference in saturation concentration (Zhao *et al.* 2014, 51). The pseudo-first-order model is mainly used in liquid/solid adsorption process. The equation is described as equation (1). (Zhao *et al.* 2013, 178)

$$\log(q_e - q_t) = \log(q_e) - \frac{k_1}{2.303} t \quad (1)$$

Where

$t$  is time [min]

$q_t$  is the amount of adsorbate adsorbed at time  $t$  [mmol g<sup>-1</sup>]

$q_e$  is the amount of adsorbate adsorbed at equilibrium [mmol g<sup>-1</sup>]

$k_1$  is rate constant [min<sup>-1</sup>]

### 3.1.2 Pseudo-second-order

Pseudo-second-order model assumes that the rate-determining step depends on chemical surface reaction. The pseudo-second-order equation is presented in equation (2). (Zhao *et al.* 2013, 178)

$$\frac{t}{q_t} = \frac{1}{k_2 q_e^2} + \frac{1}{q_e} t \quad (2)$$

Where

$t$  is time [min]

$q_t$  is the amount of adsorbate adsorbed at time  $t$  [mmol g<sup>-1</sup>]

$q_e$  is the amount of adsorbate adsorbed at equilibrium [mmol g<sup>-1</sup>]

$k_2$  is rate constant [g mmol<sup>-1</sup>min<sup>-1</sup>]

### 3.1.3 Intra-particle diffusion

In order to evaluate how diffusion affects the rate of adsorption, the intra-particle diffusion model should be used. The relative equation is shown in equation (3). (Zhao *et al.* 2013, 178)

$$q_t = k_{id} t^{1/2} + C \quad (3)$$

Where

$t$  is time [min]

$q_t$  is the amount of adsorbate adsorbed at time  $t$  [mmol g<sup>-1</sup>]

$k_{id}$  is the rate constant [ $\text{mmol g}^{-1} \text{min}^{-1/2}$ ]

$C$  represents the thickness of the boundary layer [ $\text{mmol g}^{-1}$ ]

### 3.2 Adsorption isotherm models

Isotherms describe the equilibrium between adsorption capacity and adsorbate concentration at constant temperature. Isotherms can be obtained by regression analysis based on experimental data. Isotherm equations play an important role in understanding the adsorption mechanism.

Initial adsorbate concentration will affect the adsorption capacity of an adsorbent. The adsorption capacity will increase with the increase of adsorbate concentration followed by holding the line because of saturation of active adsorbent sites. This can be explained that higher initial concentration will provide higher driving force, which can conquer the resistance of mass transfer between liquid and solid phase.

There are large numbers of isotherm models which can be used in one- or multi-component systems. The most commonly used isotherm models in adsorption of metals are Langmuir, Freundlich, Dubinin-Radushkevich, Sips, BiLangmuir, BET equations, which are applicable in one-component system. There are also some models applicable for multi-component system. These models will be introduced detailed in this chapter.

#### 3.2.1 Langmuir isotherm model

Langmuir isotherm model is based on different assumptions. The first assumption is that the surface of the adsorbent is homogeneous and uniform, which means that all the adsorption sites are equivalent. The second assumption is that adsorbed molecules do not interact with each other. Another assumption is that there is only monolayer formed during the adsorption process, which will produce competition between adsorbate molecules. Based on the theory, an equation is derived to explain the interaction between adsorption

sites on the adsorbent and the amount of adsorbate in the liquid phase. Langmuir isotherm equation is shown in equation (4). (Zhao *et al.* 2014, 52)

$$q_e = \frac{q_m K_L C_e}{1 + K_L C_e} \quad (4)$$

Where

$q_e$  is the adsorption capacity of adsorbent [mmol g<sup>-1</sup>]

$q_m$  is the maximum adsorption capacity of adsorbent [mmol g<sup>-1</sup>]

$C_e$  is the equilibrium concentration of adsorbate [mmol L<sup>-1</sup>]

$K_L$  is the affinity constant or the energy of adsorption obtained after non-linear fit [L mmol<sup>-1</sup>]

### 3.2.2 Freundlich isotherm model

Compared to Langmuir isotherm model, Freundlich isotherm assumes that the surface of the adsorbent is heterogeneous and nonuniform. Besides, multilayer adsorption is possible without saturation. Freundlich refers to non-ideal and reversible adsorption process. This model is applicable for high and middle concentration, but not for low concentration (Zhu *et al.* 2015, 416). Freundlich isotherm equation is shown in equation (5). (Zhao *et al.* 2014, 52)

$$q_e = K_F C_e^{1/n_F} \quad (5)$$

Where

$q_e$  is the adsorption capacity of adsorbent [mmol g<sup>-1</sup>]

$C_e$  is the equilibrium concentration of adsorbate [mmol L<sup>-1</sup>]

$n_F$  is the Freundlich parameter related to the degree of system heterogeneity

$K_F$  is a unit capacity coefficient [(mmol g<sup>-1</sup>)/ (L mmol<sup>-1</sup>)<sup>n<sub>F</sub></sup>]

### 3.2.3 Dubinin-Radushkevich (D-R) isotherm model

This model is more general without the assumption of homogeneous surface compared to Langmuir model (Chen *et al.* 2012, 389). It is used to distinguish between physical adsorption and chemical adsorption (Chen *et al.* 2012, 389). It is an empirical model describing adsorption both on homogeneous and heterogeneous surfaces (Zhu *et al.* 2015, 416). Moreover, this model can be suitable for high solute activities and medium range of concentration data (Zhu *et al.* 2015, 416). However, it does not behave well in asymptotic property (Zhu *et al.* 2015, 416). The linear equation of D-R model is shown in equation (6). (Chen *et al.* 2012, 389)

$$\ln q_e = \ln q_m - \beta \varepsilon^2 \quad (6)$$

Where

$q_e$  is the adsorption capacity of adsorbent [mmol g<sup>-1</sup>]

$q_m$  is the maximum amount of metal ions [mmol g<sup>-1</sup>]

$\beta$  is a constant connected with mean free energy of adsorption per mole of the adsorbate [mol<sup>2</sup>/J<sup>2</sup>]

$\varepsilon$  is the Polanyi potential [kJ<sup>2</sup>mol<sup>2</sup>]

$\varepsilon$  can be calculated by using the following equation (7).

$$\varepsilon = RT \ln\left(1 + \frac{1}{C_e}\right) \quad (7)$$

Where

$R$  is gas constant [J/(mol K)]

$T$  is temperature [K]

$C_e$  is the equilibrium concentration of adsorbate [mmol L<sup>-1</sup>]

To distinguish between physical and chemical adsorption, the mean free energy of adsorption is needed, which can be determined by the following equation (8).

$$E = 1\sqrt{-2\beta} \quad (8)$$

Where

$E$  is the mean free energy of sorption [J mol<sup>-1</sup>]

$\beta$  is a constant connected with mean free energy of adsorption per mole of the adsorbate [mol<sup>2</sup>/J<sup>2</sup>]

If the value of  $E$  is below 8 J mol<sup>-1</sup>, then the adsorption is a physical adsorption; if the value of  $E$  is between 8 and 16 J mol<sup>-1</sup>, then the adsorption is an ion exchange process; if the value of  $E$  is above 16 J mol<sup>-1</sup>, then the adsorption is a chemical adsorption. (Zhu *et al.* 2015, 417)

### 3.2.4 Sips (Langmuir-Freundlich) isotherm model

Both Langmuir and Freundlich isotherm models are too simple to explain complicated adsorption process according to different surface heterogeneity. Hence, Sips isotherm model can be applied. It is a combination of Langmuir and Freundlich isotherms, which also take heterogeneity into consideration. Sips isotherm equation is shown in equation (9). (Zhao *et al.* 2014, 52-53)

$$q_e = \frac{q_m (K_S C_e)^{n_s}}{1 + (K_S C_e)^{n_s}} \quad (9)$$

Where

$q_e$  is the adsorption capacity of adsorbent [ $\text{mmol g}^{-1}$ ]

$q_m$  is the maximum adsorption capacity of adsorbent [ $\text{mmol g}^{-1}$ ]

$C_e$  is the equilibrium concentration of adsorbate [ $\text{mmol L}^{-1}$ ]

$K_S$  is affinity constant or Langmuir equilibrium parameter [ $\text{L mmol}^{-1}$ ]

$n_s$  is related to Freundlich heterogeneity factor ( $n_s=1/n_F$ )

The validity of the chosen isotherm model can be determined quantitatively by using normalized standard deviation  $\Delta q$  (%), which is calculated from the following equation (10). (Chen *et al.* 2012, 389)

$$\Delta q(\%) = \sqrt{\frac{\sum [(q_{\text{exp}} - q_{\text{cal}}) / q_{\text{max}}]^2}{n-1}} \times 100 \quad (10)$$

Where

$q_{\text{exp}}$  is the experimental value [ $\text{mmol g}^{-1}$ ]

$q_{\text{cal}}$  is the calculated value [ $\text{mmol g}^{-1}$ ]

$q_{\text{max}}$  is the maximum amount of metal ions [ $\text{mmol g}^{-1}$ ]

$n$  is dimensionless constant

### 3.2.5 BiLangmuir isotherm model

This model assumes that there are two different kinds of adsorption sites on the adsorbent surface. There is only one layer on the adsorbent surface as Langmuir isotherm model. The main point is that these two kinds of sites have different stabilities towards the adsorbed compounds because of the interaction between the sited and the adsorbed complexes. The related equation is shown in equation (11). (Zhao *et al.* 2013, 180)

$$q_e = \frac{q_{m,1}K_1C_e}{1 + K_1C_e} + \frac{q_{m,2}K_2C_e}{1 + K_2C_e} \quad (11)$$

Where

$q_{m,1}$ ,  $q_{m,2}$  is maximum adsorption capacity of two different adsorption sites [mmol g<sup>-1</sup>]

$K_1$ ,  $K_2$  is adsorption energies related to adsorption sites 1 and 2 respectively [L mmol<sup>-1</sup>]

$C_e$  is the equilibrium concentration of adsorbate [mmol L<sup>-1</sup>]

### 3.2.6 BET (Brunauer, Emmet, Teller) isotherm model

The assumptions of this model is almost similar, however, the main difference is that this model allows multi-layer adsorption. It describes behavior close to solubility limit (liquid) or condensation (gases). It is used to characterize porous adsorbents with "BET surface". The BET equation is shown in the following equation (12). (Ladavos *et al.* 2012, 126)

$$\frac{1}{[V_{ads}(\frac{P_0}{P} - 1)]} = \frac{C-1}{V_m C} \times \frac{P}{P_0} + \frac{1}{V_m C} \quad (12)$$

Where

$V_{ads}$  is volume of gas adsorbed at standard temperature and pressure (STP) [273.15 K

and atmospheric pressure ( $1.013 \times 10^5$  Pa)] [ml]

$V_m$  is volume of gas adsorbed at STP to produce an apparent monolayer on the same surface [ml]

$P$  is partial vapour pressure of adsorbate gas in equilibrium with the surface [Pa]

$P_0$  is saturated pressure of adsorbate gas [Pa]

$C$  is dimensionless constant that is related to the enthalpy of adsorption of the adsorbate gas on the powder sample

$C$  can be calculated from the following equation (13).

$$C = \exp\left(\frac{E_1 - E_L}{RT}\right) \quad (13)$$

Where

$E_1$  is the heat of adsorption for the first layer [J]

$E_L$  is the heat of adsorption for the second or higher layers [J]

$R$  is gas constant [J/(mol K)]

$T$  is temperature [K]

### 3.2.7 Isotherm models for multi-components system

After finding out the most suitable one-component isotherm model, the competitive study of multi-components can be modeled by using the extended isotherm model of the corresponding one-component model.

To obtain the competitive study of different metals, the adsorption experiments will be

performed in multi-metal system. Normally, there are three cases in multi-metal system shown below. (Zhao *et al.* 2014, 53)

$q_{mix}/q_{one} > 1$  ( The adsorption process is promoted by the presence of other metals)

$q_{mix}/q_{one} = 1$  ( There is no observable interaction between each other)

$q_{mix}/q_{one} < 1$  ( The adsorption process is hindered by the presence of other metals)

### 3.2.8 Extended Sips isotherm model

The extended Sips model can be used to model multi-metal system. It takes interaction factors of individual component into account. The applied equation is presented in equation (14).

$$q_{ei} = \frac{q_m (K_{Si} C_{ei})^{n_{Si}}}{1 + \sum_{j=1}^N (K_{Sj} C_{ej})^{n_{Sj}}} \quad (14)$$

Where

$q_e$  is the adsorption capacity of adsorbent [mmol g<sup>-1</sup>]

$q_m$  is the maximum adsorption capacity of adsorbent [mmol g<sup>-1</sup>]

$C_e$  is the equilibrium concentration of adsorbate [mmol L<sup>-1</sup>]

$K_s$  is affinity constant [L mmol<sup>-1</sup>]

$n_s$  describes surface heterogeneity

$N$  is the number of total metals

$i$  is a particular component

$j$  represents all components

### 3.2.9 Extended BiLangmuir isotherm model

In this model, one active adsorption site can only be occupied by one ion at the same time. Therefore, a mixed monolayer will be formed on the adsorbent surface after competition between ions. The corresponding equations are presented as follows in equation (15) and (16). (Zhao *et al.* 2013, 181)

$$q_{e1} = \frac{q_{m,1,1}K_{1,1}C_{e1}}{1 + K_{1,1}C_{e1} + K_{2,1}C_{e2}} + \frac{q_{m,1,2}K_{1,2}C_{e1}}{1 + K_{1,2}C_{e1} + K_{2,2}C_{e2}} \quad (15)$$

$$q_{e2} = \frac{q_{m,2,1}K_{2,1}C_{e2}}{1 + K_{1,1}C_{e1} + K_{2,1}C_{e2}} + \frac{q_{m,2,2}K_{2,2}C_{e2}}{1 + K_{1,2}C_{e1} + K_{2,2}C_{e2}} \quad (16)$$

Where

$q_{m,1,1}$ ,  $q_{m,1,2}$  is maximum adsorption capacity of component 1 on adsorption sites 1 and 2 respectively [mmol g<sup>-1</sup>]

$K_{1,1}$ ,  $K_{1,2}$  is adsorption energies related to adsorption of component 1 on adsorption sites 1 and 2 respectively [L mmol<sup>-1</sup>]

$q_{m,2,1}$ ,  $q_{m,2,2}$  is maximum adsorption capacity of component 2 on adsorption sites 1 and 2 respectively [mmol g<sup>-1</sup>]

$K_{2,1}$ ,  $K_{2,2}$  is adsorption energies related to adsorption of component 2 on adsorption sites 1 and 2 respectively [L mmol<sup>-1</sup>]

$C_{e1}$ ,  $C_{e2}$  is the equilibrium concentration of component 1 and 2 [mmol L<sup>-1</sup>]

### 3.3 Adsorption capacity and desorption ratio

The adsorption capacity is calculated from the following formula. (Yao 2010, 184)

$$q_e = \frac{(C_i - C_e)V}{m} \quad (17)$$

Where

$q_e$  is adsorption capacity [mmol g<sup>-1</sup>]

$C_i$  is initial concentration of metal ions in solution [mg L<sup>-1</sup>]

$C_e$  is equilibrium concentration of metal ions in solution [mg L<sup>-1</sup>]

$V$  is total volume of solution [L]

$m$  is the mass of adsorbent [g]

The distribution coefficient is calculated from the following equation. (Yao 2010, 184)

$$D = \frac{q_e}{C_e} \quad (18)$$

Where

$D$  is distribution coefficient [L g<sup>-1</sup>]

$q_e$  is adsorption capacity [mg g<sup>-1</sup>]

$C_e$  is equilibrium concentration of metal ions in solution [mg L<sup>-1</sup>]

Desorption ratio can be calculated from the following equation. (Yao 2010, 184)

$$E(\%) = \frac{(C_d V_d)}{(C_i - C_e)V} \times 100\% \quad (19)$$

Where

$E$  is desorption ratio

$C_d$  is the concentration of metal ions in the desorption solution [ $\text{mg L}^{-1}$ ]

$V_d$  is the volume of the desorption solution [L]

$C_i$  is initial concentration of metal ions in solution [ $\text{mg L}^{-1}$ ]

$C_e$  is equilibrium concentration of metal ions in solution [ $\text{mg L}^{-1}$ ]

$V$  is total volume of solution [L]

#### **4 Analytical methods for determining REEs in liquid phase and characterization methods for adsorbents**

It is very important to choose reliable analytical method in determining the concentration of REEs in the samples. There are several methods, which can be used. Inductively coupled plasma optical emission spectrometry (ICP-OES), inductively coupled plasma mass spectrometry (ICP-MS), isotope dilution mass spectrometry and neutron activation analysis are the most popular analytical methods (Pasinli *et al.* 2005, 42). However, ICP-OES is the most frequently used method in determining the concentration of metal ions and it is also used in this study.

##### **4.1 Inductively Coupled Plasma-Optical Emission Spectrometry (ICP-OES)**

ICP-OES is a multivariate method for removal interference from major components in real samples to determine concentration of the major component. Basically, ICP-OES has three advantages: (1) the emission lines of minor component will be shown separately with the major component without separation beforehand like chromatography and electrophoresis; (2) the use of different lines for different components facilitates the identification of the sample; (3) due to each component has many emission lines with various intensities, it is possible to identify the sample over a wide concentration range. (Ito *et al.* 1998, 241)

Inductively coupled plasma (ICP) is the light source of atomic emission spectroscopy. The theory of this method is that when it is under thermal excitation or electrical excitation state, different atoms emit different characteristic spectrum, which can be used to distinguish different atoms and estimate the compositions, furthermore to make qualitative and quantitative analysis. As for the determination of lower than 1% component, the detection limit is ppm.

The characteristic spectrum is formed when the excited state atom transit back to ground state. The ground state is low energy state. The excited state is high energy state and unstable. Thus the excited state atoms will release energy in the form of radiation and transit

back to ground state. Because of the differences in energy level structure, the emission spectrum characteristics of different atoms are different. Therefore, the qualitative study can be achievable. Because of the differences in atom concentrations, the emission intensities are different. Therefore, the quantitative analysis can be performed.

Normally, there are three main parts in ICP spectrometer. The first one is light source system. In this part, the sample will be evaporated into gaseous atom with the energy provided by light source and then produce ray radiation. The second part is light splitting system. The compound light from light source is divided by monochromator into spectrum in order of the wavelength. The last part is detecting system. The wavelength and intensity of spectrum will be detected by the detector.

There are advantages and disadvantages in using ICP. In addition to high sensitivity, good selectivity, fast analysis speed, less sample consuming, it is suitable for analysis of micro-sample and trace inorganic components. It is widely used in metals, mineral and alloy. However, it is not possible to detect nonmetal elements. The error will be increased with the increase of concentration.

The used quantitative analysis method is standard curve method, which is very suitable for large number of samples. The standard solutions with different concentrations are prepared based on the standard solution of the components to be tested. Under the same chromatographic conditions and same sample volumes, the peak area or peak height is detected. Then the standard curve can be drawn with peak area or peak height versus sample concentration. The standard curve should go through the origin; otherwise, there are systematic errors. The samples should be tested under the same chromatographic conditions when the standard curve is drawn. Then the peak area or peak height is measured based on which the concentration can be checked through the standard curve.

#### **4.2 Inductively Coupled Plasma-Mass Spectrometry (ICP-MS)**

ICP-MS is another analytical method to determine elements. It is capable to detect mainly

metals and several nonmetals. It has many advantages compared to other elemental analysis techniques such as atomic absorption and emission spectrometry including ICP-AES. The advantages are: (1) It has equal or better detection limits for most elements than Graphite Furnace Atomic Absorption Spectroscopy (GFAAS); (2) it has higher throughput than GFAAS; (3) it can handle both simple and complex matrices with minimum matrix interferences due to the high temperature of ICP source; (4) It has superior detection capability to ICP-AES under the same sample throughput; (5) it has ability to obtain isotropic information. (Wolf E. R. 2005)

ICP-MS is composed of ICP torch, interface unit and mass spectrometer. The used source is inductively coupled plasma same as ICP-AES. The torch is composed of three quartz socket tube layers, where carrier gas, auxiliary gas and cooling gas flows are introduced from inside to outside of the layers. The upper part of torch is placed induction coils, which will be supplied with radio-frequency electric current to produce magnetic field perpendicular to coils.

The argon gas is ionized by an electric spark for a short time to introduce free electrons to the gas stream. The free electrons will collide with other argon atoms to produce more electrons, which will form vortex. The temperature is really high, therefore the argon gas turn to be plasma with the temperature around 10,000 K. The samples will be introduced into the plasma and then evaporated, decomposed, excited and ionized. The auxiliary gas is used to maintain the plasma with amount of 1 L min<sup>-1</sup>. The cooling gas is introduced to the outside tube to produce spiral airflow, which will cool the inwall of coil tubes down. The flowrate of cooling gas is about from 10 to 15 L min<sup>-1</sup>.

The most common way to introduce the sample is to use concentric or angle type pneumatic nebulizer to produce aerosol, which can be sprayed with carrier gas into torch. The sample size is about 1 mL min<sup>-1</sup>.

Since the temperature of torch is about 8000 k to the top of the coil 10 mm, elements with

lower than 7 eV ionization energy can be ionized completely; only more than 20% elements can be ionized with ionization energy lower than 10.5 eV. As most important elements have lower than 10.5 eV ionization energy, it has very high sensitivity. Also elements with high ionization energy can be detected, however, the sensitivity is quite low.

### **4.3 Characterization methods used for adsorbents**

In this thesis work, many methods were used to characterize adsorbents properties. FTIR spectroscopy type Nicolet Nexus 8700 (USA) was used to determine functional groups on the surface of adsorbents before and after rare earth ions binding. The elemental analyses for relevant adsorbents were carried out with an Elementar Vario ELIII elemental analyzer (Germany) and the results were used to determine the loading of cross-linkers (EDTA) on  $\beta$ -CD in this case. The morphologies of adsorbents were characterized on a Jeol JSM-5800 scanning electron microscope (SEM) equipped with a Thermo Scientific Ultra Dry SDD Energy dispersive X-ray spectrometer (EDS). Elemental mapping was performed by Energy dispersive X-ray spectrometer (EDS) simultaneously during SEM test to identify REEs distribution on the surface of adsorbents after adsorption. The surface charge and a point of zero charge of relevant adsorbents were performed by isoelectric point titration as a function of pH by using Zetasizer Nano ZEN3500 (Malvern, UK). The zeta potential measurements were performed in 0.1 M NaCl. The stability and content of adsorbents were identified by thermogravimetric analysis (TGA) NETZSCH STA 409 TG-DTA (Germany).

### **4.4 Other used methods**

The chemical oxygen demand (COD) detection was used to detect the difference in chemical oxygen demand before and after adsorption for both two kinds of seawater from Mexico and Helsinki respectively. A Dr. Hach Lange 2800 system was used in this work.

## 5 Adsorbents used in adsorption of REEs

Various materials can be used as adsorbents. However, the adsorption results such as selectivity and capacity may be different. The regeneration is also a very important criterion in choosing adsorbents. Good regeneration means the adsorbents can be easily regenerated without any substantial decline in adsorption capacity. Regeneration ability represents the reusability of the adsorbents, which is really significant from economical point of view. Generally, adsorbents should be applicable in large-scale industry applications, which requires good selectivity, stability and low cost.

### 5.1 Adsorbents used in this research

$\beta$ -cyclodextrin ( $\beta$ -CD) is a seven-unit cyclic oligosaccharide produced from the enzymatic degradation of starch. It has gained vast attention as efficient and selective adsorbent in a large amounts of areas (Fuhrer *et al.* 2011, 1924-9). The most important property of CDs is their geometrically well-defined cavities, which are useful for host-guest inclusion interactions with a wide range of molecules of suitable size and polarity (Yu *et al.* 2008, 7522-7). CDs are well-known to reliably form rapid and reversible inclusion complexes with various nonpolar organic molecules (Sobocinski *et al.* 2014, 3575-86) rely on their host-guest interactions feature (Fuhrer *et al.* 2011, 1924-9), especially aromatic molecules (Schofield *et al.* 2012, 1645-1653; Crini 2003. 193-8). In this case, the high density of hydroxyl groups besides the CD cavities could serve as the coordination sites to form complexes with various metal ions (Zhu *et al.* 2015, 413). Furthermore, the hydroxyl groups can be modified with various functional groups such as carboxylate groups, endowing the CDs with extra specific properties (Yu *et al.* 2008, 7522-7).

Due to the high water solubility of CDs and their derivatives (Fuhrer *et al.* 2011, 1924-9), they have to be immobilized on an insoluble support (Schofield *et al.* 2012, 1645-1653), or to be cross-linked to obtain CD polymers (CDP) adsorbents. (Liu *et al.* 2011, 3499-511; Wilson *et al.* 2013, 271-7) EDTA, a chelating agent, is widely used to maintain metal ions

as a hexadentate ligand (two amines and four carboxylate groups). EDTA also have the potential to modify CD to functionalize the obtained CD derivative with higher uptake capacity and selectivity for the target metals (Zhao *et al.* 2013, 174-182). In the previous study, EDTA-modified chitosan and/or silica has been successfully used to remove Co(II) and Ni(II) from contaminated water (Zhao *et al.* 2013, 174-182). Recently, J. Michel *et al.* have synthesized an EDTA-linked  $\beta$ -CD dimer as a chemical sensor by the reaction of EDTA anhydride with mono-(propylamino)-appended  $\beta$ -CD to form strong complexes with Lanthanide(III) ions (Michel *et al.* 2002, 2056–2064). However, the EDTA-linked  $\beta$ -CD dimer is water-soluble, thus it is limited to be used as adsorbent in liquid medium. In addition, the synthesis method is complex and not green because several organic solvents are involved.

More recently, EDTA-, ethylene glycol tetraacetic acid (EGTA)-, and diethylene triamine pentaacetic acid (DTPA)-functionalized chitosan biopolymers have been successfully synthesized as cross-linkers (Zhao 2015, 1271-1281; Repo *et al.* 2010, 73-82; Zhao *et al.* 2013, 174-182). This cross-linking method has greatly enhanced the adsorption abilities towards metals. As comparison, epichlorohydrin (EPI), another cross-linker, has been reported to have high level of toxicity and carcinogenicity to human beings and animals (Hirakawa *et al.* 2014, 431-432; Zeiger *et al.* 2005, 136-151). Moreover, in comparison with EPI, EDTA is relatively cheaper and lower toxicity (Zhao *et al.* 2015, 1271-1281). Therefore, in this work we synthesized EDTA- $\beta$ -CD in a proper way and used it as adsorbent towards REEs. EPI-cross-linked  $\beta$ -cyclodextrin (EPI- $\beta$ -CD) was also synthesized and characterized as comparison with EDTA- $\beta$ -CD.

EDTA- $\beta$ -CD polymer was obtained by polycondensation reaction of  $\beta$ -CD with EDTA. The reaction is shown in Figure 1. In this reaction, the primary hydroxyl groups of  $\beta$ -CD have priority to be esterified with the carboxyl groups of EDTA, since the reaction was carried out in aqueous solution (Zhao *et al.* 2009, 125-130). However, when an excessive amount of EDTA are used, the secondary hydroxyl groups as well as the primary hydroxyl groups of CDs will react with the carboxyl groups, even in the aqueous solution (Kawano *et al.* 2014, 8094-8100). Water could be evaporated away very quickly during the reaction process

because Petri dish (the container) was wide open and the reaction temperature was high. Then the water generated during the polycondensation reaction was instantly taken away, then the reaction equilibrium was pushed forward, resulting in a network EDTA-cross-linked  $\beta$ -CD polymer.

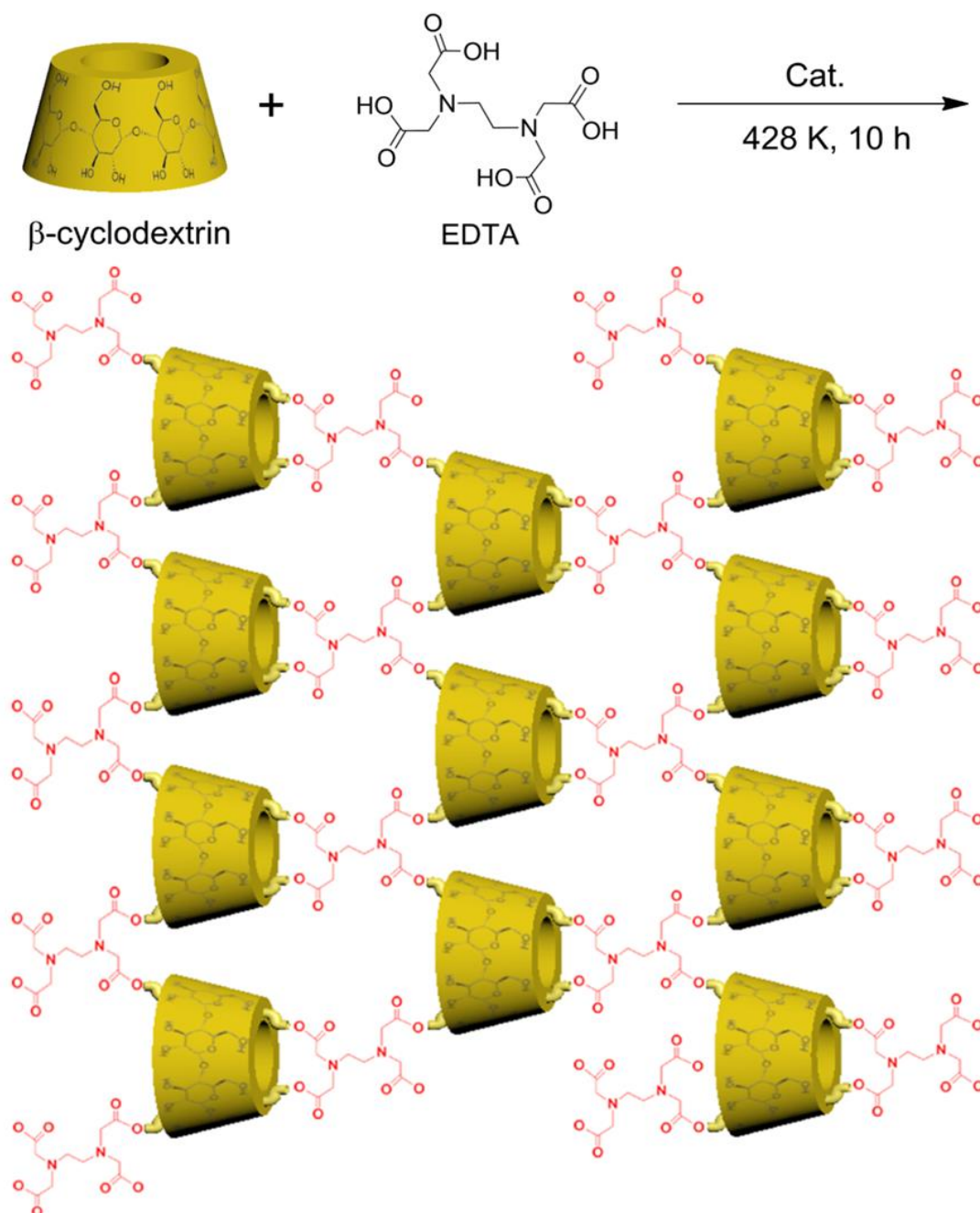


**Figure 1.** Synthesis of EDTA-cross-linked  $\beta$ -cyclodextrin (EDTA- $\beta$ -CD) polymer.

## 6 Experimental testing

All reagents were purchased from Sigma-Aldrich (Finland) and were used without further purification.  $\beta$ -CD were 97+% pure and all other chemicals were analytical grade. Stock solutions of 1000 mg L<sup>-1</sup> were prepared via dissolving appropriate amounts of metal nitrate salts in deionized water. Working solutions ranging from 10 to 500 mg L<sup>-1</sup> of metals were prepared by diluting the stock solutions. Adjustment of pH was undertaken using 0.1 M NaOH/HNO<sub>3</sub>. Deionized water (18.2  $\Omega$ ) was used throughout the whole experiments.

### 6.1 ICP

According to chapter 4, the most suitable, simple and reliable analytical method for detecting metal ions is ICP-OES, which is also achievable in Green Chemistry Laboratory for this work. Therefore, in the experimental part, ICP-OES is the mainly used analytical equipment.

In this work, an ICP-OES Model Icap 6300 (Thermo Electron Corporation, U.S.A.) was used to determine concentration of REEs as shown in Figure 2. The auto sampler is Cetac ASX-260. The cooler should be open 20 mins before use. Normally, the rinse nitric acid is used to wash. Some operating parameters are shown in the Table 3.

**Table 3.** Operating parameters for ICP

ICP operation parameters	
RF power	1150 W
Pump rate	50 rpm
Auxiliary gas flow	1.0 L/min
Nebulizer gas flow	on
Purge gas flow	Normal



**Figure 2.** The figure of ICP-AES used in this work.

## 6.2 Preparation of adsorbents

EDTA- $\beta$ -CD polymer was synthesized from the esterification-polycondensation method by reacting 4 g of  $\beta$ -CD with 6 g of EDTA with the catalysis of  $\text{Na}_2\text{HPO}_4$  at 155 °C for 10 h. EPI- $\beta$ -CD was also synthesized as a blank control.

**Synthesis of EDTA- $\beta$ -CD.** EDTA- $\beta$ -CD polymers were synthesized by reacting  $\beta$ -CD with EDTA as a cross-linker and sodium dihydrogen phosphate (MSP) as a catalyst by reference to a previous report on the preparation of citric acid cross-linked  $\beta$ -CD polymers (Zhao *et al.* 2009). Dried  $\beta$ -CD (4 g, 3.5 mmol), EDTA (6 g, 20.4 mmol), MSP ( $\text{Na}_2\text{HPO}_4 \cdot 7\text{H}_2\text{O}$ , 2.68 g, 10 mmol) and 20 mL of deionized water were mixed in a round bottom flask and stirred in a 100 °C oil bath for 1 h. Polyethylene glycol 200 (PEG-200, 0.5 g, 2.5 mmol) as dispersant was added dropwise to help dissolve  $\beta$ -CD in water. The mixture was transferred into a Petri dish ( $\phi$ 160 mm) and heated in an oven at 155 °C for 10 h. After cooling at room temperature, the resulting condensation polymer product was ground and soaked with 500

mL of deionized water, and then suction filtered and rinsed with a large amount of 0.1 M HCl, deionized water, 0.1 M NaOH, again deionized water, and methanol, to remove the unreacted materials and catalyst. The final product was dried in vacuum at 60 °C overnight. The resulting products are shown in Figure 3.



**Figure 3.** Image of synthesized adsorbents.

**Synthesis of EPI- $\beta$ -CD.** As comparison, an insoluble EPI- $\beta$ -CD polymer was synthesized according to a typical procedure by using EPI as a cross-linker under an alkaline environment (Gidwani *et al.* 2014, 130-7; Liu *et al.* 2011, 3499-511).

### **6.3 Preparation of samples**

The specific calculated amount of europium (III) nitrate hydrate ( $\text{Eu}(\text{NO}_3)_3 \cdot 5\text{H}_2\text{O}$ ), cerium (III) nitrate hydrate ( $\text{Ce}(\text{NO}_3)_3 \cdot 6\text{H}_2\text{O}$ ) and lanthanum (III) nitrate hydrate ( $\text{La}(\text{NO}_3)_3 \cdot 6\text{H}_2\text{O}$ ) were weighted through balance, 2.8169 g, 3.099 g and 3.117 g respectively. Then they were added to 1000 mL flask to obtain the 1000 mg L<sup>-1</sup> for Eu(III), Ce(III) and La(III) stock

solutions by the addition of deionized water. The stock solutions were transferred to mild-mouth bottles for storage and further usage.

### 6.3.1 Samples preparation for pH studies

The initial concentration of samples ( $C_i$ ) was decided to be  $100 \text{ mg L}^{-1}$  by diluting of the stock solutions. The 50 mL flasks were used to adjust pH and obtain  $100 \text{ mg L}^{-1}$  samples. The calculated amount of stock solution (5 mL) was added to seven 50 mL flasks for each Eu(III) and Ce(III) samples paralleled. Nitric acid was used to adjust pH. The samples were preset with different pH from 1 to 5. The pH of samples should not be over 7 to avoid hydroxide formation, which will lead to precipitation. The amount of added nitric acid is empirical according to the previous experimental experience. The amount of added nitric acid and the measured real pH values by pH meter are shown in Table 4. After adjusting pH with nitric acid, the 50 mL flasks were filled with deionized water. Finally, the samples were transferred from 50 mL flasks to 50 mL reagent bottles ready for use.

**Table 4.** Designed pH ranges of samples.

Preset pH	1	2	2.5	3	3.5	4	5
Real pH	0.97	2.04	2.496	3.064	3.529	4.053	5.383
Amount of used $\text{HNO}_3$	4mL 1 M $\text{HNO}_3$	0.4mL 1 M $\text{HNO}_3$	0.13mL 1 M $\text{HNO}_3$	0.4mL 0.1 M $\text{HNO}_3$	0.13mL 0.1 M $\text{HNO}_3$	0.04mL 0.1 M $\text{HNO}_3$	no acid addition

### 6.3.2 Samples preparation for contact time studies

The pH is determined based on the results of pH study. Finally, the optimum pH is defined to be 4. The initial concentration is determined to be  $200 \text{ mg L}^{-1}$  ( $1.33 \text{ mmol L}^{-1}$ ) in this case. The time interval is designed as shown in Table 5. Firstly, 20 ml of  $1000 \text{ mg/L}$  of Eu(III),

Ce(III) and La(III) were added to three 100 ml flasks. Then 0.08ml of 0.1 M HNO<sub>3</sub> was added to each flasks to adjust pH to the desired value. Finally, deionized water was added to three flasks to reach 100 ml. Then the prepared 200 mg/L samples were transferred to three reagent bottles and sealed.

**Table 5.** Different contact time for Eu(III), Ce(III) and La(III)

t [min]	2	5	10	15	30	45	60	90	120	240	360	>1200
---------	---	---	----	----	----	----	----	----	-----	-----	-----	-------

### 6.3.3 Samples preparation for different initial concentrations

The pH was still adjusted to 4 according to the method shown in chapter 6.3.1. The contact time was set to be more than 20 h. The initial concentrations are shown in Table 6. The corresponding amount of 1000 mg L<sup>-1</sup> Eu(III), Ce(III) and La(III) stock solution was taken into five 50 mL flasks. Then 0.04 mL 0.1 M HNO<sub>3</sub> was added to adjust pH. Finally, deionized water was added to reach 50 mL. Then solutions were transferred into 15 reagent bottles and sealed.

**Table 6.** Different initial concentration with the added amount of stock solution of Eu(III), Ce(III) and La(III)

Preset Ci [mg L <sup>-1</sup> ]	10	20	50	150	300
The added amount of stock solution[mL]	0.5	1	2.5	7.5	15

### 6.3.4 Samples preparation for Multi-component REE systems studies

The competitive study with different initial concentration was also performed. The samples were prepared by diluting the previous prepared samples. The data is shown in Table 7.

**Table 7.** The preparation of competitive study with different initial concentration

The target concentration [mg L <sup>-1</sup> ]	The added previous samples [mL]				
5	20 mg L <sup>-1</sup> La(III)	20 mg L <sup>-1</sup> Ce(III)	20 mg L <sup>-1</sup> Eu(III)	Deionized water	0.1 M HNO <sub>3</sub>
	4	4	4	4	-
15	50 mg L <sup>-1</sup> La(III)	50 mg L <sup>-1</sup> Ce(III)	50 mg L <sup>-1</sup> Eu(III)	Deionized water	0.1 M HNO <sub>3</sub>
	5	5	5	1.66	-
50	150 mg L <sup>-1</sup> La(III)	150 mg L <sup>-1</sup> Ce(III)	150 mg L <sup>-1</sup> Eu(III)	Deionized water	0.1 M HNO <sub>3</sub>
	5	5	5	-	-
100	300 mg L <sup>-1</sup> La(III)	300 mg L <sup>-1</sup> Ce(III)	300 mg L <sup>-1</sup> Eu(III)	Deionized water	0.1 M HNO <sub>3</sub>
	5	5	5	-	-
200	1000 mg L <sup>-1</sup> La(III)	1000 mg L <sup>-1</sup> Ce(III)	1000 mg L <sup>-1</sup> Eu(III)	Deionized water	0.1 M HNO <sub>3</sub>

	2	2	2	4	0.06
--	---	---	---	---	------

Taking the first one as example, 4 mL of 20 mg L<sup>-1</sup> La(III), Ce(III), Eu(III) and deionized water were added into one reagent bottle. Then 5 mg L<sup>-1</sup> of La(III), Ce(III) and Eu(III) sample was obtained with total volume of 16 mL.

### 6.3.5 Samples preparation for preconcentration of REEs studies from pure water, tap water and seawater

Pure water, tap water, and sea water matrices were tested. Two kinds of seawater were used for preconcentration experiments in this study. The S<sub>1</sub> seawater was taken at a depth of 1 m from the Gulf of Finland near Helsinki. The S<sub>2</sub> seawater collected from Gulf Stream in the Gulf of Mexico, was purchased from Sigma-Aldrich. Both the seawater samples were membrane-filtered (0.45 µm) and disinfected under ultraviolet radiation by an 8 W UV-C lamp (output: 2.5 W UV; length: 287 mm; diameter: 15.5 mm). Chemical oxygen demand (COD) was detected by using a Dr. Hach Lange 2800 system.

All samples were spiked with La(III), Ce(III), and Eu(III) to final concentrations of 1.0 µg L<sup>-1</sup>. 0.5 mL 1000 mg L<sup>-1</sup> standard La(III), Ce(III) and Eu(III) solutions were taken to four 500 mL flasks and then filled the flasks with different tested matrices to get 1 mg L<sup>-1</sup> samples. Then 1mL of the above solutions were taken into four 1000 mL flasks and then filled again with same matrices to get 1.0 µg L<sup>-1</sup> samples.

### 6.4 Batch adsorption

The batch experiments of La(III), Ce(III), and Eu(III) sorption onto EDTA-β-CD adsorbent were carried out by mixing 10 mg of adsorbent with 5 mL of REE solutions (dose: 2 g L<sup>-1</sup>) at designated concentrations ranging from 0.05 to 2.0 mmol L<sup>-1</sup>. All the tests were conducted in duplicate.

#### 6.4.1 Adsorption in mono-component system

All the sample tubes were sealed and shaken in a shaker for sufficient long time for pH study. For the study of contact time, the tubes were shaken for different contact time according to the time span shown in the above table 9.

After adsorption, the samples were filtered by using 0.45  $\mu\text{m}$  polypropylene syringe filter. For the study of contact time, the filtration was done separately for each sample according to the fixed contact time. The supernatant liquor were filtered into new tubes and sealed. The filtration process is followed by a dilution process, which is very important for the following ICP analysis. Because ICP analysis cannot analyze samples with very high concentration.

1 mL of filtrate with the equilibrium concentration  $C_e$  was taken into new tube, and then 9 ml 2.5%  $\text{HNO}_3$  was added to each tube to dilute the filtrate 10 times. 2.5%  $\text{HNO}_3$  was prepared by diluting 35 mL 65%  $\text{HNO}_3$  into 1000mL flask. The solutions after dilution were the final samples for ICP analysis, which were used to determine the equilibrium concentration  $C_e$ .

Meanwhile, samples before adsorption were also diluted to determine the initial concentration  $C_i$  by using ICP-AES accurately, which was done in every adsorption study. In this case this sample was chosen randomly among all the samples before adsorption regardless of pH differences.

However, the dilution process was slightly different for the study of different initial concentrations. The detailed dilution processes are presented in Table 8.

**Table 8.** Same dilution process for samples after filtration and samples before filtration

Samples [mg $\text{L}^{-1}$ ]	10	20	50	150	300
----------------------------------	----	----	----	-----	-----

Dilution	3 mL filtrate+ 3 mL HNO <sub>3</sub>	3 mL filtrate+ 3 mL HNO <sub>3</sub>	2 mL filtrate+ 8 mL HNO <sub>3</sub>	1 mL filtrate+ 9 mL HNO <sub>3</sub>	0.5 mL filtrate+ 9.5 mL HNO <sub>3</sub>
----------	---	---	---	---	--

#### 6.4.2 Adsorption in Multi-component REE systems

The competitive adsorption study of La(III), Ce(III), and Eu(III) onto EDTA- $\beta$ -CD adsorbent were conducted in multi-component systems, containing the same initial concentration of each kind of REE ranging from 0.03 to 1.33 mmol L<sup>-1</sup> (from 10 to 300 mg L<sup>-1</sup>). The molar ratio of La(III), Ce(III), and Eu(III) were set to be 1:1:1. To maximize the adsorption capacities of REEs by the adsorbent, the initial pH value of 4.0 was used in this study according to the results from mono-component system. To reach the adsorption equilibrium, an excessive contact time of 20 h was used for the multi-component systems. The process was similar to mono-component system.

#### 6.4.3 Preconcentration of REEs studies from pure water, tap water and seawater

Amount of 400 mL REEs samples with different matrices were mixed with 0.4 g of EDTA- $\beta$ -CD (dose: 1g L<sup>-1</sup>) and agitated in a rotary oscillator at 150 rpm at ambient temperature for 10 h. Afterwards the adsorbents were separated by vacuum filtration and rinsed with 40 mL of water..

After adsorption, the adsorbents were separated from the solution by vacuum filtration (0.45  $\mu$ m) separately. And then the adsorbents were transferred into reagent bottles to be centrifuged. After centrifuge, the supernatant liquid were poured away and then the adsorbents were dried in oven until no obvious liquor can be seen. During the whole after-adsorption treatment process, the loss of adsorbents was tried to be avoided.

Subsequently, REEs were eluted by using 4 mL of 2 M HNO<sub>3</sub>. Then the supernatant was

separated with adsorbents by centrifuge. The concentrated samples (100 fold) were analyzed by ICP. All the adsorbents were mixed in one bottle and then washed twice by 30 mL of 2 M HNO<sub>3</sub> and deionized water and finally once by acetone. After washing, the adsorbents were dried in oven for sufficient time and recycled.

### 6.5 Preparation standard solutions for ICP

The standard solutions (1000 mg L<sup>-1</sup>) of Eu(III) and Ce(III) are off the shelf. In order to prepare standard solution with different concentrations, different amount of standard solution (1000 mg L<sup>-1</sup>) was taken to be diluted to the target concentration in 50 mL flasks. The target concentration and the added amount of standard solution are shown in Table 9. Taking the first target concentration as an example, 1 mL of 1000 mg L<sup>-1</sup> Eu(III) standard solution, 1 mL of 1000 mg L<sup>-1</sup> Ce(III) standard solution and 1 mL of 1000 mg L<sup>-1</sup> La(III) standard solution were taken into 50 mL flasks. Then 5% HNO<sub>3</sub> was added to dilute the standard solution to 50 mL. As a result, the final concentration was 20 mg L<sup>-1</sup>.

With the samples of different standard concentrations, the standard curve in which concentration versus peak area or peak height can be made. The initial concentration ( $C_i$ ) and equilibrium concentration ( $C_e$ ) can be determined from the standard curve.

**Table 9.** Different concentrations of standard solution for ICP and the corresponding additions.

The target concentration [mg L <sup>-1</sup> ]	20	10	5	2	0.5	0.1	4 (for calibration)
The added amount of standard solution	1 mL of 1000 mg L <sup>-1</sup>	0.5 mL of 1000 mg L <sup>-1</sup>	0.25 mL of 1000 mg L <sup>-1</sup>	0.1 mL of 1000 mg L <sup>-1</sup>	2.5 mL of 10 mg L <sup>-1</sup> diluted	0.5 mL of 10 mg L <sup>-1</sup> diluted	0.2 mL of 1000 mg L <sup>-1</sup>

## 7 Results for experimental testing

### 7.1 Characterizations of EDTA- $\beta$ -CD and EPI- $\beta$ -CD

Here EPI-cross-linked  $\beta$ -cyclodextrin (EPI- $\beta$ -CD) is compared to EDTA-cross-linked  $\beta$ -cyclodextrin (EDTA- $\beta$ -CD) for the following characterization studies.

The quantitative elemental analyses are presented in Table 10. The EDTA content in EDTA- $\beta$ -CD could be calculated based on N content in EDTA- $\beta$ -CD because all the N content of EDTA- $\beta$ -CD comes from EDTA molecules (no N element in  $\beta$ -CD). Furthermore, the  $\beta$ -CD content could be calculated by the exclusion of EDTA content from EDTA- $\beta$ -CD. The calculations are listed below in Table 10. As a result, the composition of EDTA- $\beta$ -CD was of 64.53% EDTA (2.21 mmol g<sup>-1</sup>) and 35.47% for  $\beta$ -CD (0.31 mmol g<sup>-1</sup>). Compared to EPI- $\beta$ -CD (9.02) reported before (Liu *et al.* 2011, 3499-511), EDTA- $\beta$ -CD has lower cross-linking degree. However, considering the amount of cross-linking terminals of the used cross-linkers (two for EPI and four for EDTA), the cross-linking degree of EDTA- $\beta$ -CD should be two-fold of EPI- $\beta$ -CD. (Zhao *et al.* 2015, 1271-1281) The high cross-linking degree made the  $\beta$ -CD polymers water insoluble.

**Table 10.** Elemental analysis results of  $\beta$ -CD and EDTA- $\beta$ -CD

Sample	Elemental content (wt.%)				EDTA content (mmol g <sup>-1</sup> )	CD content		Degree of cross-linking
	N	C	H	S		wt.%	mmol g <sup>-1</sup>	
$\beta$ -CD	0	39.07	6.47	0	0			
EPI- $\beta$ -CD	0	47.76	7.06	0	0			
EDTA- $\beta$ -CD	6.19	41.73	5.52	0	2.21 <sup>a</sup>	35.47 <sup>b</sup>	0.31 <sup>c</sup>	7.07 <sup>d</sup>

<sup>a</sup> Calculated from nitrogen content:  $EDTA\ content = (6.19\% * 1000\ mg\ g^{-1}) / (M_{Nitrogen} * 2)$ ;

<sup>b</sup> Calculated from EDTA content:  $CD\ content = (1000\ mg - 2.21\ mmol * M_{EDTA}) / 1000\ mg * 100\%$ ;

<sup>c</sup> Converted according to  $CD\ content = 35.47\% * 1000\ mg\ g^{-1} / M_{CD}$ ;

<sup>d</sup> Calculated according to  $n_{EDTA} / n_{CD} = 2.21\ mmol\ g^{-1} / 0.31\ mmol\ g^{-1}$ .<sup>4</sup>

In addition, SEM (Figure 4 a and b) images presented obvious differences of the morphologies between EPI- $\beta$ -CD and EDTA- $\beta$ -CD, smooth for EPI- $\beta$ -CD and rough for EDTA- $\beta$ -CD. EDX results (Figure 4 c and d) showed a good agreement with results of Elemental analysis in Table 10. The much higher Na content of EDTA- $\beta$ -CD than EPI- $\beta$ -CD might be attributed to the  $-\text{COONa}$  groups on its surface.

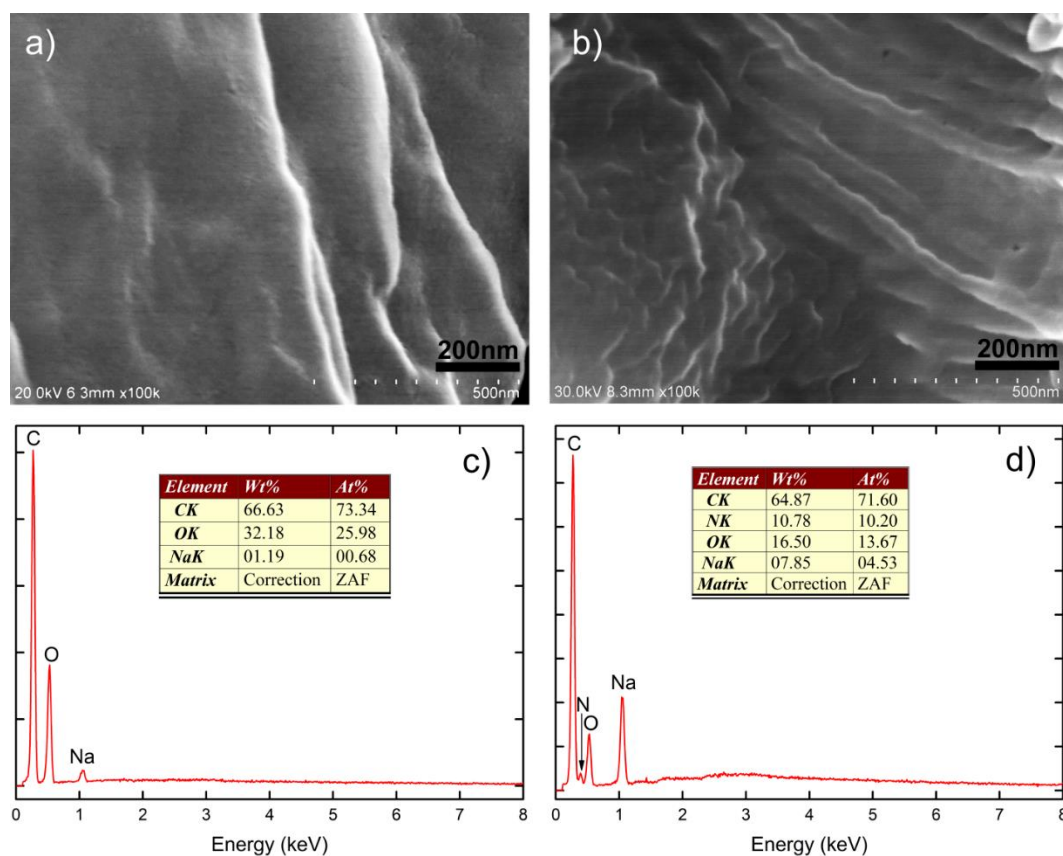


**Figure 4.** SEM images and EDX spectra of EPI- $\beta$ -CD (a, c) and EDTA- $\beta$ -CD (b, d).

Zeta potentials of CD polymers measured at different pH are shown in Figure 5. The isoelectric point was determined as 2.23 for EDTA- $\beta$ -CD, much lower than 4.42 for EPI- $\beta$ -CD (Badruddoza *et al.* 2011, 1177-86; Konkena *et al.* 2012, 12432-7). This might be

attributed to the existence of EDTA groups on the surface of EDTA- $\beta$ -CD (Zhao *et al.* 2015, 1271-1281).

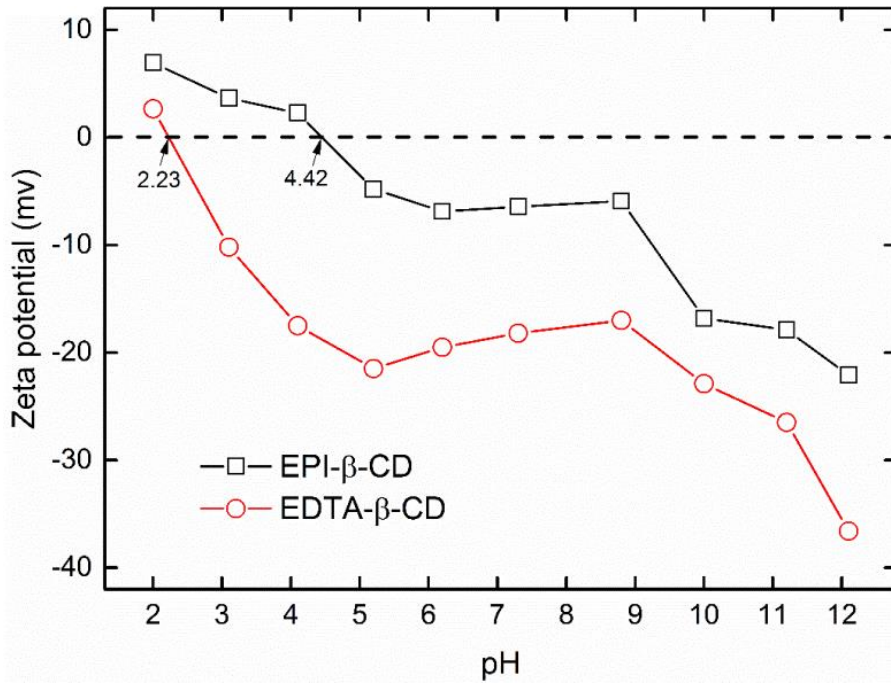


**Figure 5.** Zeta potentials of EPI- $\beta$ -CD and EDTA- $\beta$ -CD as a function of solution pH.

The thermos stabilities of EDTA- $\beta$ -CD and EPI- $\beta$ -CD were measured by TGA. The weight percentage versus temperature are shown in Figure 6. Compared to EPI- $\beta$ -CD polymer, the stability of EDTA- $\beta$ -CD decreased, which might arise from the existence of EDTA groups. The curve of EDTA- $\beta$ -CD indicated three weight losses at temperature range of 60-110 °C, 170-270 °C, and 270-930 °C, which responded to water loss, EDTA decomposition (Zhao *et al.* 2015, 1271-1281) and  $\beta$ -CD decomposition (Li *et al.* 2015, 55-62) respectively.

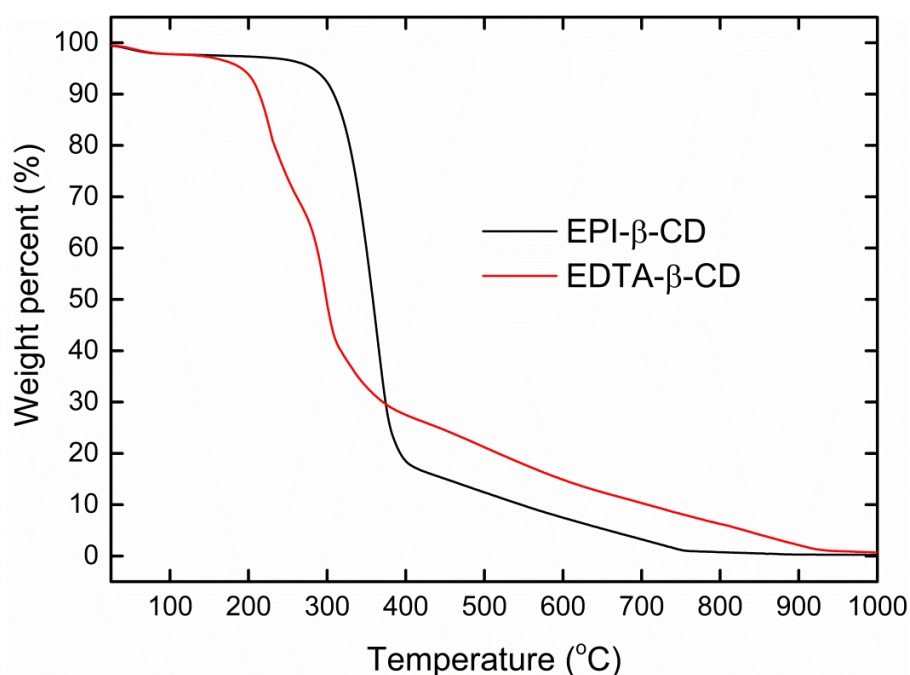


**Figure 6.** TGA curves of EPI-β-CD and EDTA-β-CD.

## 7.2 Effects of pH

The pH of liquid phase is an important parameter in adsorption process because the protonation of surface functional groups and the degree of ionization of the cations are strongly pH-dependent (Hokkanen *et al.* 2013, 40-47). To maximize the uptake of REEs by adsorbents, identification of an optimum pH is very necessary. The influence of pH on the adsorption of REEs was investigated for EDTA-β-CD, and compared with EPI-β-CD. The results are shown in Figure 7.

Similar to other EDTA-modified materials, the adsorption of REEs was found to be dependent on pH. At pH 1 the adsorption capacity was quite low, which might due to the electrostatic repulsions between the surface of the adsorbent and RE ions. Later, the adsorption soared with increasing pH from 2 to 3 and afterwards reached an equilibrium gradually. This result is in good agreement with the isoelectric point of EDTA-β-CD at pH 2.23. The uptake of RE ions was limited after pH 4, which might due to the ligand loading saturation. Therefore, pH 4.0 was chosen as the optimum pH for the subsequent adsorption tests to maximize REEs uptake.

It is worthy to note that the adsorption efficiency of REEs by EDTA- $\beta$ -CD was much higher than that of EPI- $\beta$ -CD, indicating that EDTA groups may play a major role in adsorption. However, the adsorption by EPI- $\beta$ -CD still occurred (close to 0.1 mmol g<sup>-1</sup>, Figure 7), therefore, rare earth ions might be coordinated with the high density of hydroxyl groups besides the CD cavities and captured in the dense  $\beta$ -CD networks of EPI- $\beta$ -CD. It is noted that the low adsorption capacity at lower pH can be used to regenerate adsorbent. Indeed, the adsorption process is reversible and desorption can be achieved by treatment with acid.

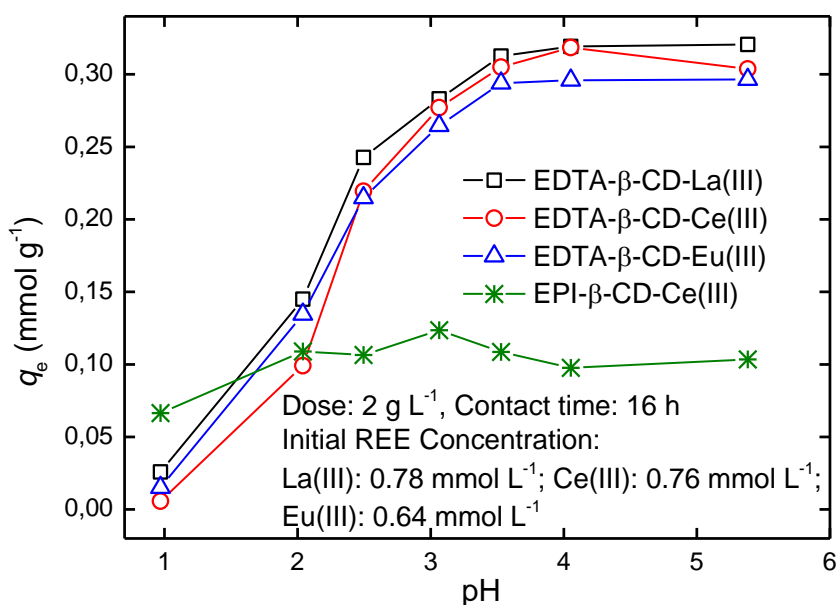


**Figure 7.** Effect of pH on adsorption of La(III), Ce(III), and Eu(III) onto EDTA- $\beta$ -CD adsorbent.

### 7.3 Effect of contact time and adsorption kinetics

In order to determine the equilibration time for the maximum uptake of REEs and the adsorption rate, the adsorption amounts of La(III), Ce(III), and Eu(III) onto EDTA- $\beta$ -CD were investigated as a function of time and the results were depicted in Figure 8 and inset. It is seen that the adsorption rate was quite fast at the beginning and could attain more than 40% and 80% of maximum adsorption capacity within 2 min and 45 min, respectively. The fast adsorption rate observed in this study is consistent with the previous studies on the

adsorption of Cd(II) and Pb(II) by EDTA-functionalized chitosan (Zhao *et al.* 2013, 174-182) and it might be due to large number of available adsorption sites for REEs on the adsorbent surface (2.21 mmol g<sup>-1</sup> EDTA coverage). Moreover, the adsorption gradually reached equilibrium within 240 min for La(III), Ce(III) and Eu(III) due to the adsorption sites were occupied by RE ions and reached saturation. Therefore, contact time of 4 h was chosen for all the further adsorption experiments.

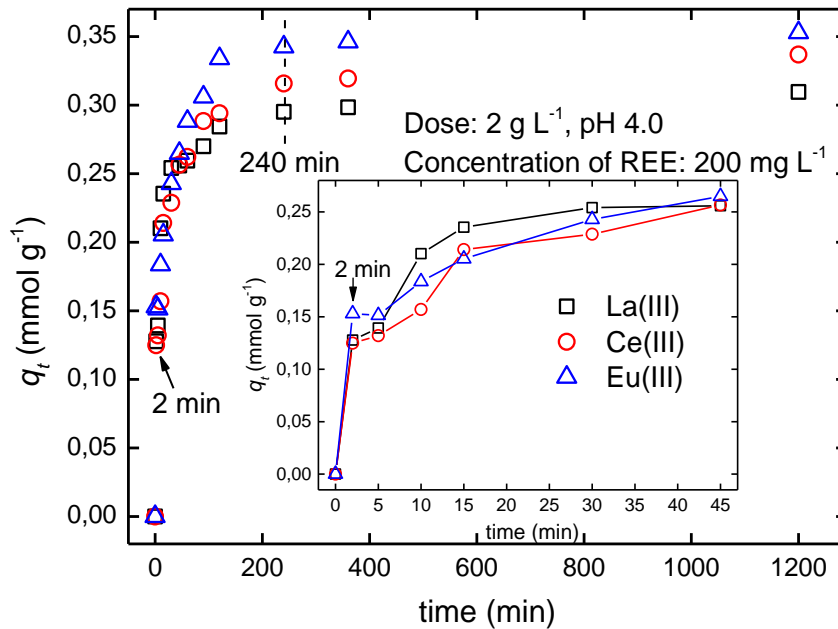


**Figure 8.** Effect of contact time on La(III), Ce(III), and Eu(III) adsorption by EDTA-β-CD (Inset: time range of 0-45 min).

In order to evaluate the adsorption rate and rate-determining step such as mass transfer and chemical reaction, pseudo-first-order, pseudo-second-order model and intra-particle diffusion were used to simulate the experimental data. The kinetic plots of REEs onto EDTA-β-CD is presented in Figure 9 and the calculated kinetic constants are shown in Table 11. All these results indicate that the pseudo-second-order model fits the experimental data much better than that of pseudo-first-order model. Firstly, the  $q_{e,cal}$  values calculated by pseudo-second-order model were much closer to the experimental data. Secondly,

correlation coefficients ( $R^2$ ) calculated for pseudo-second-order model are much higher than that in pseudo-first-order. Moreover, the linear pseudo-second-order curves almost fit to the experimental dots perfectly, while pseudo-first-order model failed. The failure of pseudo-first-order model might be attributed to the fact that this model is only suitable for describing the data measured near the equilibrium (Zhao *et al.* 2013, 178). All the results suggest that chemical sorption was the rate-determining step of the adsorption process and mass transfer was not involved in the adsorption mechanism (Hokkanen *et al.* 2013, 40-47). It can also be seen from  $k_2$  values that adsorption kinetics of La(III) and Eu(III) are faster than that of Ce(III) which is in good agreement with the results of adsorption rate presented in Figure 8.

As shown in Figure 9c, the illustrated three linear portions on the plots of adsorption amounts versus the square root of time indicates multi-step diffusion occurred during the adsorption of REEs onto EDTA- $\beta$ -CD. The first slope referred to external film or boundary layer diffusion between liquid surface and adsorbent surface. The second slope was attributed to the diffusion of ions in macropores and regions. The third slope was assigned to micropore diffusion. As shown in Table 11, the  $k_{id,1}$  values are much greater than those of  $k_{id,2}$  and  $k_{id,3}$ , suggesting that from bulk solution to the exterior surface of adsorbents might be the rate controlling step in this adsorption process. The relatively low values of  $k_{id,2}$  and  $k_{id,3}$  (close to zero) might be due to the difficulties for ions to reach adsorption sites because of the crosslinking between the surface groups indicating that pore diffusion was not obvious in this process and the adsorption attained equilibrium (Zhao *et al.* 2015. 1271-1281).

**Table 11.** Kinetic data for REEs adsorption by EDTA- $\beta$ -CD.

REE	$q_{e,exp}$ (mmol g <sup>-1</sup> )	Pseudo-first-order			Pseudo-second-order			Intra-particle diffusion		
		$q_{e,cal}$ (mmol g <sup>-1</sup> )	$k_1$ (min <sup>-1</sup> )	$R^2$	$q_{e,cal}$ (mmol g <sup>-1</sup> )	$k_2$ (g mmol <sup>-1</sup> min <sup>-1</sup> )	$R^2$	$k_{id,1}$ (mmol g <sup>-1</sup> min <sup>-0.5</sup> )	$k_{id,2}$ (mmol g <sup>-1</sup> min <sup>-0.5</sup> )	$k_{id,3}$ (mmol g <sup>-1</sup> min <sup>-0.5</sup> )
La(III)	0.310	0.111	0.041	0.726	0.311	0,367	0.999	0.059	0.005	7.41×10 <sup>-4</sup>

Ce(III)	0.337	0.158	0.039	0.795		0.339	0,218	0.999		0.050	0.009	0.001
Eu(III)	0.353	0.165	0.055	0.864		0.356	0,268	0.999		0.108	0.020	$7.08 \times 10^{-4}$

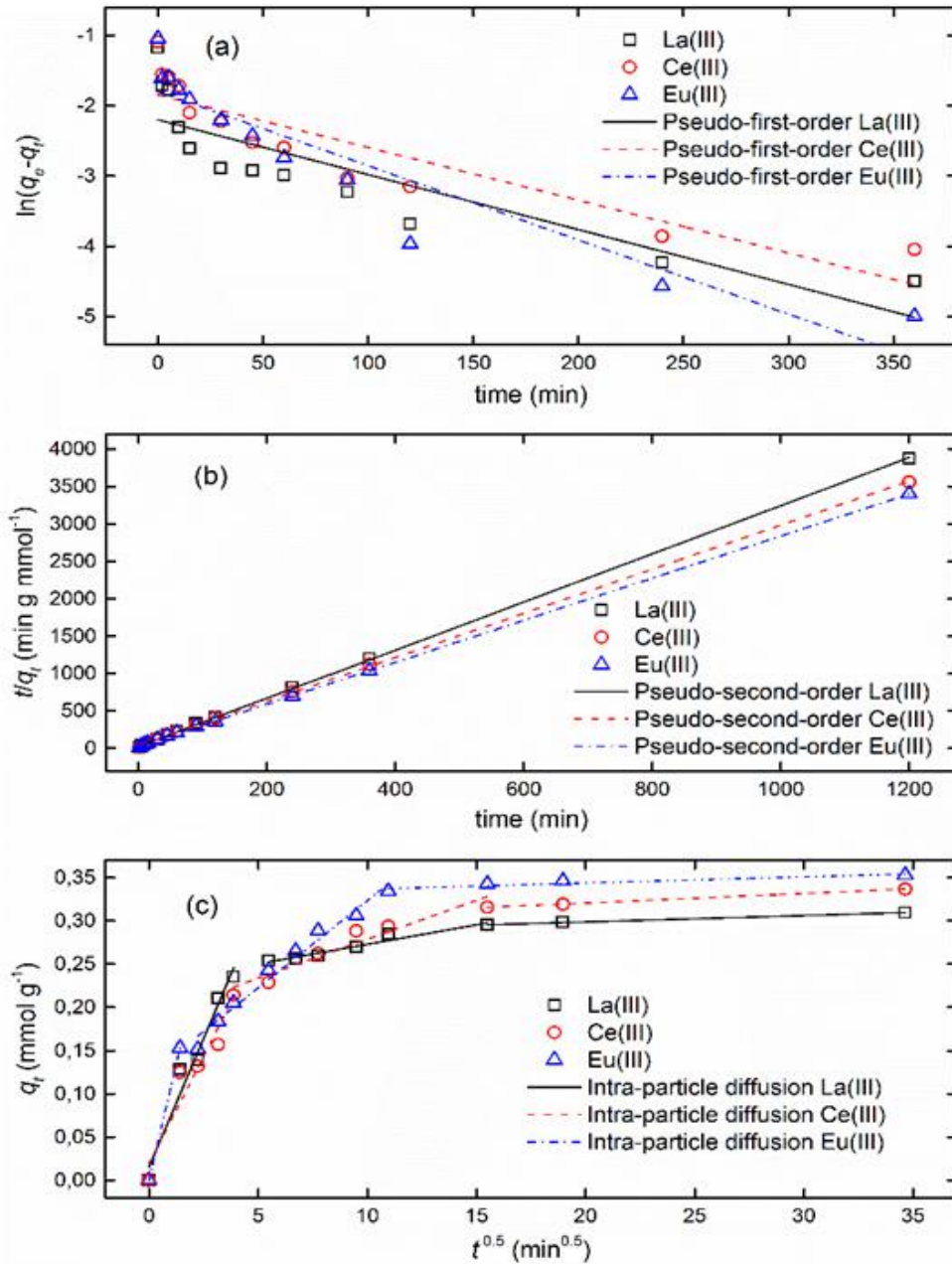


**Figure 9.** Kinetic modeling of REEs adsorption by EDTA-β-CD.

#### 7.4 Adsorption isotherm

In order to understand the adsorption mechanism of homogeneous or heterogeneous

system deeper, adsorption isotherms should be investigated. Searching for an equilibrium model well fitted to the experimental data is significant in this work. In this work, the Langmuir, Freundlich and Sips equations were fitted to the experimental data by non-linear regression for one-component equilibrium system. The specific equations were shown in chapter 3.2. The plots of isotherms and isotherm constants are presented in Figure 10 and Table 12.

Figure 10 shows that the Langmuir model curves fit the experimental data much better than Freundlich and Sips for La(III), Ce(III) and Eu(III). From Table 12, it is seen that the correlation coefficient ( $R^2$ ) values of Langmuir model are much higher than Freundlich and Sips. Besides, the estimated adsorption capacity ( $q_m$ ) values of Langmuir model are much closer to the experimental values than others. Despite high value of  $R^2$ , the Sips model could not be presentative enough to model one-component adsorption equilibrium of La(III), Ce(III) and Eu(III) because the calculated  $q_m$  values could not correspond well to the experimental  $q_m$  values as shown in Table 12. The Freundlich model did not fit well to the experimental data according to much lower value of  $R^2$  than that of Langmuir and Sips model. Therefore, the isotherm fittings follow the order of Langmuir > Sips > Freundlich according to  $R^2$  values,  $q_m$  values and curve fitting.

A good agreement between experimental data and Langmuir model implies that the adsorption on the surface of EDTA- $\beta$ -CD is a homogeneous and all adsorption sites are equivalent. This result proves the hypothesis proposed by some researchers that  $\beta$ -CD do not adsorb RE ions through inclusion interaction (Zhao *et al.* 2013, 174-182). Thus EDTA groups can be considered to provide adsorption sites alone. According to the result obtained from elemental analysis that the coverage of EDTA on the surface of EDTA- $\beta$ -CD is 2.21 mmol g<sup>-1</sup> and the result that the observed adsorption capacity is from 0.343 to 0.365 mmol g<sup>-1</sup>, we can conclude that only 15.52 to 16.52% of adsorption sites on EDTA groups are occupied by RE ions. The values of occupation ratio is relatively lower than that of heavy metals (50.05 to 56.15%) (Zhao *et al.* 2013, 174-182), and it might be attributed to the lower stability constants ( $\log K$ ) of lanthanide-EDTA complexes than that of heavy metal-EDTA

complexes (Zhao *et al.* 2013, 174-182). It is worthy to note that the  $q_m$  values of RE ions follow the order of La(III) < Ce(III) < Eu(III). This might also be explained by their stability constants. The stability constants of EDTA complexes are 15.5 for La(III)-EDTA complexes, 15.9 for Ce(III)-EDTA<sup>-</sup> complexes, 17.3 for Eu(III)-EDTA complexes respectively (Durand *et al.* 2000, 705-714; Kawabe 2014). It is noted that the stability constants of the lanthanide EDTA complexes increase with atomic number.

**Table 12.** Isotherm constants for the one-component adsorption of REEs onto EDTA- $\beta$ -CD.

Model	REE	$q_{m,exp}$ (mmol g <sup>-1</sup> )	$q_m$ (mmol g <sup>-1</sup> )	$K_{L/F}$ (L mmol <sup>-1</sup> )	$n_F$	$R^2$
Langmuir	La(III)	0.343	0.344	41.146		0.982
	Ce(III)	0.353	0.358	29.849		0.998
	Eu(III)	0.365	0.366	28.932		0.997
Freundlich	La(III)	0.343		0.338	4.019	0.873
	Ce(III)	0.353		0.347	3.831	0.889
	Eu(III)	0.365		0.384	3.476	0.864
Model	REE	$q_{m,exp}$ (mmol g <sup>-1</sup> )	$q_m$ (mmol g <sup>-1</sup> )	$K_s$ (L mmol <sup>-1</sup> )	$n_s$	$R^2$
Sips	La(III)	0.343	0.332	56.072	1.647	0.967
	Ce(III)	0.353	0.351	33.179	1.142	0.981
	Eu(III)	0.365	0.352	51.626	2.122	0.949

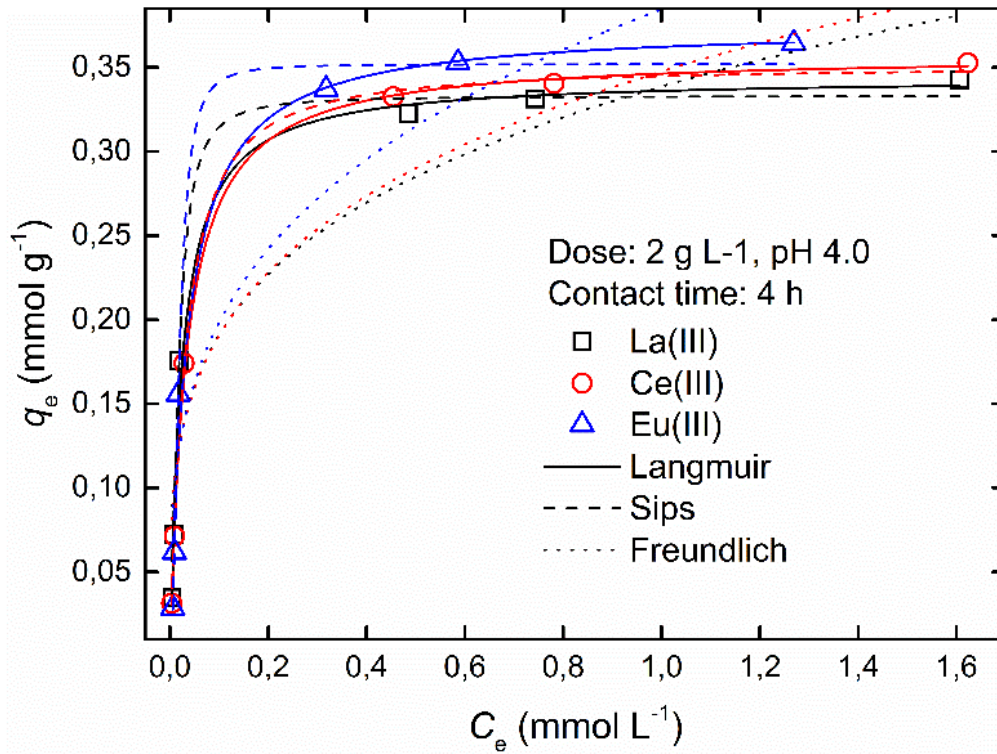


**Figure 10.** Adsorption isotherms of La(III), Ce(III), and Eu(III) on EDTA- $\beta$ -CD

The following Table 13 compares the maximum adsorption capacities of La(III), Ce(III), and Eu(III) on other used adsorbents and EDTA- $\beta$ -CD. The relatively higher values for EDTA- $\beta$ -CD than other adsorbents indicate that EDTA- $\beta$ -CD is an effective adsorbent for REEs adsorption.

**Table 13.** Comparison of maximum adsorption capacities of REEs by different adsorbents.

Adsorbents	Maximum metal adsorption capacity (mmol g <sup>-1</sup> )			References
	La(III)	Ce(III)	Eu(III)	
Hydroxyapatite	0.006	-	0.002	Granados <i>et al.</i> 2012
Platanus orientalis leaf powder	0.206 <sup>a</sup>	0.229 <sup>a</sup>	-	Sert <i>et al.</i> 2008, 13–18
TiO <sub>2</sub>	0.004 <sup>a</sup>	-	-	Li <i>et al.</i> 2004, 2248-51
SnO <sub>2</sub> - TiO <sub>2</sub> NCs	0.47 <sup>a</sup>	-	-	Rahman <i>et al.</i> 2014, 1964
Crab shell particles	-	1.034 <sup>a</sup>	0.326 <sup>a</sup>	Vijayaraghavan <i>et al.</i> 2010

Crab shells powder	-	-	0.02 <sup>a</sup>	Cadogan <i>et al.</i> 2014, 232
Brown marine alga	1.08	1.05	0.87	Vijayaraghavana <i>et al.</i> 2011, 54-59
Inmobilized pseudomonas aeruginosa	0.342	-	-	Tan <i>et al.</i> 2009, 3115–3121
BaCO <sub>3</sub>	-	-	0.1	Granados & Jiménez. 2011, 2360-2366
HPC-g-PAA/APT granular hydrogels	1.67 <sup>a</sup>	-	-	Zhu <i>et al.</i> 2015, 413
Citrate-coated magnetic nanoparticles	0.5	-	0.5	Ngomsik <i>et al.</i> 2012, 1
Magnetic GMZ Bentonite	0.13 <sup>a</sup>	-	0.17 <sup>a</sup>	Wu <i>et al.</i> 2012, 87
MgFe-LDH-A	3.46 <sup>a</sup>	-	-	Gasser & Aly. 2013, 32
HESI-SBA-15	0.06 <sup>a</sup>	-	-	Tadjarodi <i>et al.</i> 2014, 113
Biosorbents of animal (fish scales)	1.44 <sup>a</sup>	-	-	Das <i>et al.</i> 2014, 40
Bioadsorbents of plant origin (neem sawdust)	1.15 <sup>a</sup>	-	-	Das <i>et al.</i> 2014, 40
HylBA	-	-	0.83 <sup>a</sup>	Awual <i>et al.</i> 2013, 313
Chitosan nanoparticles	-	-	0.75 <sup>a</sup>	Cadogan <i>et al.</i> 2014, 232
di(2-thylhexly) phosphoric acid immobilized magnetic GMZ Bentonite	-	-	0.27 <sup>a</sup>	Chen <i>et al.</i> 2012, 387
D151 resin	-	2.798 <sup>a</sup>	-	Yao 2010, 183
mesoporous optical conjugate adsorbent	-	1.37 <sup>a</sup>	-	Awual <i>et al.</i> 2013, 327
EDTA-β-CD	0.343	0.353	0.365	this study

<sup>a</sup> Converted from the original unit of mg g<sup>-1</sup> presented in the literatures.

## 7.5 Adsorption in multi-component systems

To investigate the competitive effect of RE ions, the adsorption of multi-component system was conducted. Based on the three cases in multi-component system mentioned in chapter 3.2.7, all the obtained values of  $q_{mix}/q_{one}$  in this study were observed less than 1, indicating that the adsorption of La(III), Ce(III), and Eu(III) were hindered by the existence of each

other. The values of La(III) (0.12) and Ce(III) (0.20) are much lower than Eu(III) (0.55) suggesting that La(III) and Ce(III) were much easier to be affected by the presence of other RE ions. The inhibition between RE ions could be interpreted by Pearson law that the competition among the studied RE ions occurs because they belong to the same classification (hard metals) (Pearson 1963, 3533–3539).

An extended Sips model was applied in multi-component isotherm modeling as mentioned in chapter 3.2.8. In this study, the equation 14 can be decomposed into the following three equations in a ternary system.

$$q_{e1} = \frac{q_{m1}(K_{S1}C_{e1})^{n_{S1}}}{1+(K_{S1}C_{e1})^{n_{S1}}+(K_{S2}C_{e2})^{n_{S2}}+(K_{S3}C_{e3})^{n_{S3}}} \quad (20)$$

$$q_{e2} = \frac{q_{m2}(K_{S2}C_{e2})^{n_{S2}}}{1+(K_{S1}C_{e1})^{n_{S1}}+(K_{S2}C_{e2})^{n_{S2}}+(K_{S3}C_{e3})^{n_{S3}}} \quad (21)$$

$$q_{e3} = \frac{q_{m3}(K_{S3}C_{e3})^{n_{S3}}}{1+(K_{S1}C_{e1})^{n_{S1}}+(K_{S2}C_{e2})^{n_{S2}}+(K_{S3}C_{e3})^{n_{S3}}} \quad (22)$$

where  $q_{m1}$ ,  $K_{S1}$ ,  $n_{S1}$ ,  $q_{m2}$ ,  $K_{S2}$ ,  $n_{S2}$ , and  $q_{m3}$ ,  $K_{S3}$ ,  $n_{S3}$ , are model parameters for the three kinds of REEs respectively. The calculation was performed by using Microsoft Office Excel 2013 software. All the isotherm parameters were calculated by the solver of minimizing the Sum of the Squares of the Errors (ERRSQ) (Hokkanen *et al.* 2013, 40-47).

The experimental plots of adsorption capacity as a function of equilibrium concentrations are depicted in Figure 11. It can be seen from Figure 11 that the extended Sips model fitted the experimental data well. According the calculated values in Table 14, both the low ERRSQ value and close values of  $q_{e,exp}$  and  $q_{e,cal}$  confirm that the extended Sips model was very applicable for this three-component system. Compared to the result in one-component system, all the parameters were affected by the competition.

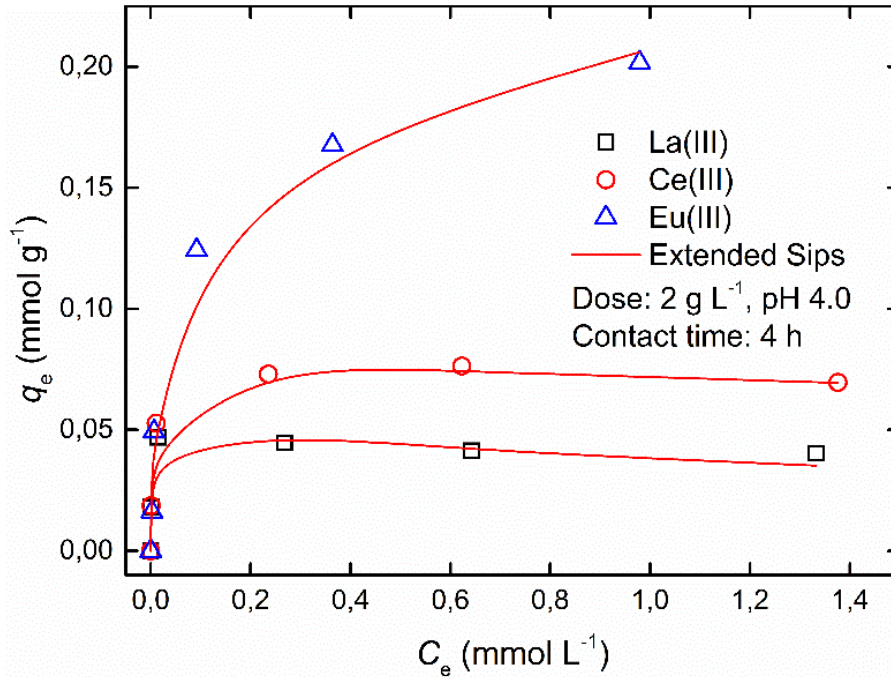


**Figure 11.** Modeling of three-component system of La(III), Ce(III) and Eu(III) adsorption on EDTA- $\beta$ -CD by using the extended Sips model.

**Table 14.** Constants for the three-component adsorption of La(III), Ce(III) and Eu(III) adsorption on EDTA- $\beta$ -CD.

REE	$q_{e,exp}$ (mmol g <sup>-1</sup> )	$q_{e,cal}$ (mmol g <sup>-1</sup> )	$K_s$ (L mmol <sup>-1</sup> )	$n_s$	ERRSQ
La(III)	0.041	0.035	0.595	4.075	0.049
Ce(III)	0.070	0.068	2.554	2.949	
Eu(III)	0.202	0.205	6.625	1.829	

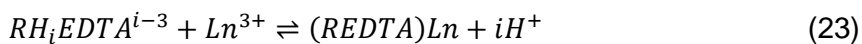
It is worthy to be noted that the differences of adsorption capacity among all the studied RE ions were expanded compared to one-component system. The advantage of Eu(III) was obvious in three-component system following the order Eu(III)  $\gg$  Ce(III)  $>$  La(III) while in one-component system following the order Eu(III)  $>$  Ce(III)  $>$  La(III). This kind of trend has been observed by Vijayaraghavan for a four-component system of La, Ce, Eu and Yb, where the resulted adsorption capacity in four-component system follow the order of Eu(III)  $>$  Ce(III)  $>$  La(III)  $>$  Yb(III), however in one-component system it was in the order of La(III)  $>$  Ce(III)  $>$  Eu(III)  $>$  Yb(III). This affinity sequence difference was explained by using water

structure constants by the authors that lower value of water structure constant leads to higher affinity (Vijayaraghavana *et al.* 2011, 54-59). Overall, the affinity difference between REEs can be due to the combined effects of water structure constant and stability constant.

## 7.6 Adsorption mechanism

In adsorption, several sorption mechanism, such as electrostatic interaction, chelation and complexation, could be used to explain the sorption (Luo *et al.* 2014. 145–155). According to the Figure 6, the result that the isoelectric point was 2.23 for EDTA-β-CD proved the existence of immobilized carboxylate groups in FTIR characterization study. At pH < 2.23, the surface of EDTA-β-CD is positive repelling the trivalent cations. However, carboxylate groups were deprotonated at pH > 2.23 which will increase the negative charge of the material. Consequently, the electrostatic interaction between negative surface of material and positive RE ions will facilitate adsorption. This should be considered one of the adsorption mechanism.

Based on thermodynamic data, EDTA has various species distribution represented by  $H_nEDTA^{n-4}$ , where n ranges from 1 to 5. The calculation by MINEQL software (MINTEQA ver. 3.0) showed that the negatively charged  $H_3EDTA^-$ (10%) and  $H_2EDTA^{2-}$ (90%) were the primary species at pH 4, where most of the experiments were conducted. Therefore, the REEs adsorption by EDTA-β-CD could be expressed by following equation:



Where  $R$  represent β-CD and  $i$  is the number of hydrogen ions complexed with EDTA ranging from 2 to 3, while  $Ln^{3+}$  is the target metal (Nash *et al.* 2012. 14547-14556). The above equation suggest that chelation and complexation are significant for the adsorption.

In order to understand the adsorption mechanism further, the FTIR spectra of EDTA-β-CD before and after adsorption of RE ions is presented in Figure 12. It is obvious that the  $\nu(C=O)$  band at  $1674\text{ cm}^{-1}$  shifted to  $1599\text{ cm}^{-1}$  and the bands of  $\nu(-OH)$  and tertiary amine at  $3342$

$\text{cm}^{-1}$  were weakened due to the interaction between carboxylate and amine groups in EDTA and RE ions (Zhao *et al.* 2015, 1271-1281).

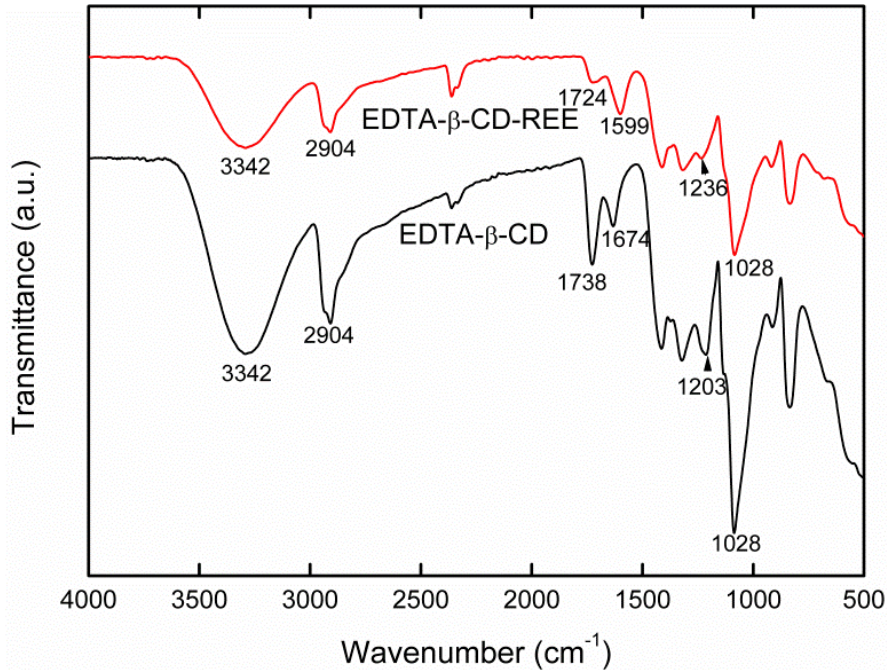


**Figure 12.** FTIR spectra of EDTA- $\beta$ -CD before and after the adsorption of La(III), Ce(III) and Eu(III).

The distribution of La(III), Ce(III), and Eu(III) on EDTA- $\beta$ -CD can be characterized by EDS mapping after adsorption. The EDS spectrum of EDTA- $\beta$ -CD and elemental distribution on EDTA- $\beta$ -CD are depicted in the Figure 13. It confirmed the presence of RE ions on the surface of EDTA- $\beta$ -CD. The signal pots on the surface demonstrated that RE ions were evenly loaded on the surface adsorption sites of EDTA- $\beta$ -CD and further proved the adsorption sites were well constructed and distributed. Take La(III) as an example: the distribution of La(III) on EDTA- $\beta$ -CD surface is in the range of 0% to 2.81%. The image of La(III) showed that the adsorption of La(III) is 0% in the dark blue zones and 2.81% in the red zones. The maximum loaded amount of La(III), Ce(III) and Eu(III) on EDTA- $\beta$ -CD followed the order Eu(III) > Ce(III) > La(III), which was consistent with the previous result.

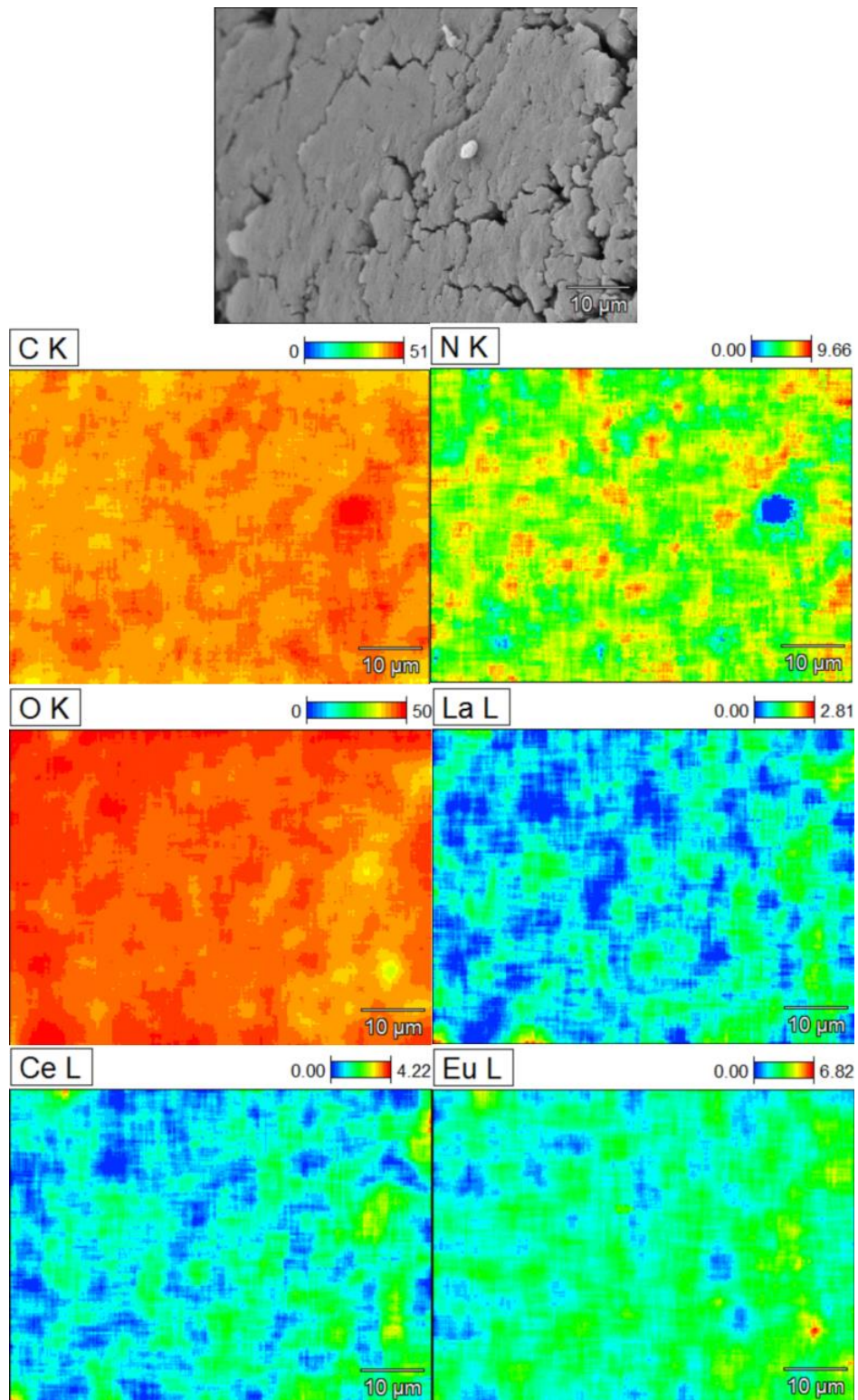


**Figure 13.** SEM image and the EDS elemental distribution mapping of EDTA-β-CD after adsorption of REEs (initial concentration: 200 mg L<sup>-1</sup> La(III), Ce(III) and Eu(III)).

### 7.7 Preconcentration of REEs studies from pure water, tap water and seawater

Preconcentration is a very important application for adsorbents. As the fact that the determination of RE ions in seawater is quite difficult because the concentration is below the detection limit of instruments (Liang *et al.* 2005, 125–129). The amount of  $1 \mu\text{g L}^{-1}$  RE ions were spiked before preconcentration (Wen *et al.* 1999, 621-626). The determination limits and the concentrations after preconcentration are presented in Table 15. According to the literature (Wen *et al.* 1999, 621-626), the determination limits were calculated based on the way that three times the standard deviation of 10 runs of blank solutions.

It is seen from Table 15 that the determination limits of the four tested matrices followed the order of pure water < tap water < S<sub>1</sub> seawater (Gulf of Finland) < S<sub>2</sub> seawater (Gulf of Mexico). S<sub>2</sub> seawater is much higher than S<sub>1</sub> seawater might due to the higher surface salinity of S<sub>2</sub> seawater (32‰) than that of S<sub>1</sub> seawater (6‰) according to the data from International Council for the Exploration of the Sea (Anon. ICES), Oceanographic Database. Moreover, the concentration of REEs after preconcentration were increased a lot compared to the determination limits. The recoveries of the matrix solutions were conducted precisely (84-105%). Overall, this preconcentration method was proved to be effective and reliable. During the preconcentration process, the adsorbents were regenerated by treating with 2 M HNO<sub>3</sub>.

**Table 15.** The determination limits and 100-fold preconcentration of REEs in various matrices.

REE	Spiked concentration ( $\mu\text{g L}^{-1}$ )	Determination limit ( $\mu\text{g L}^{-1}$ )				Determined after preconcentration ( $\mu\text{g L}^{-1}$ )			
		Pure water	Tap water	S <sub>1</sub> seawater	S <sub>2</sub> seawater	Pure water	Tap water	S <sub>1</sub> seawater	S <sub>2</sub> seawater
La(III)	1.0	0.9	1.9	2.8	6.4	92.8	97.9	84.9	90.6
Ce(III)	1.0	7.3	12.5	16.1	22.6	100.0	93.3	94.5	105.2
Eu(III)	1.0	0.2	0.6	1.0	4.3	94.8	89.4	90.9	102.3

## 8 Conclusion

A novel adsorbent (EDTA- $\beta$ -CD) for REEs adsorption was successfully synthesized by a simple and green approach via the polycondensation reaction of  $\beta$ -CD with EDTA. The adsorbents was characterized. The adsorption behavior of La(III), Ce(III) and Eu(III) onto EDTA- $\beta$ -CD was successfully investigated. The maximum adsorption capacities were obtained. The effect of pH and contact time were determined. The kinetics and isotherm models were found according to the experimental data. The adsorption mechanism of La(III), Ce(III) and Eu(III) onto EDTA- $\beta$ -CD were discussed.

EDTA has high coverage (64.53%, 2.21 mmol EDTA presented in 1 g of the resulting EDTA- $\beta$ -CD) on the surface of EDTA- $\beta$ -CD and the high crosslinking degree of EDTA (7.07) endowed the  $\beta$ -CD water insolubility. EDTA- $\beta$ -CD was effective on the adsorption of La(III), Ce(III) and Eu(III). The maximum REEs uptake was 0.310 mmol g<sup>-1</sup> for La(III), 0.337 mmol g<sup>-1</sup> for Ce(III) and 0.353 mmol g<sup>-1</sup> for Eu(III) respectively.

The effect of pH on the adsorption of La(III), Ce(III) and Eu(III) onto EDTA- $\beta$ -CD was investigated. Obviously, the adsorption capacity of La(III), Ce(III) and Eu(III) on EDTA- $\beta$ -CD was strongly pH-dependent. Similar to previous research, the adsorption efficiency was low when pH was extremely low, on the other hand, this fact made desorption available. To obtain maximum uptake of rare earth ions, the optimum pH was determined to be 4.

The fast adsorption equilibrium could be attained in 240 min, suggesting that this adsorbent can be used in practical application. The result of initially fast adsorption rate confirmed again the previous explanation that because of large amounts of available adsorption sites. The kinetics complied with the pseudo-second-order model indicating that chemical sorption was the rate-determining step and the rate of adsorption was also affected by intra-particle diffusion. The adsorption rate of studied rare earth ions followed this order: La(III)>Eu(III)>Ce(III). The rate controlling step was the moving of rare earth ions from bulk

solution to exterior surface of adsorbent and pore diffusion was not significant in adsorption process.

The isotherm study of adsorption equilibrium complied with Langmuir model indicating the homogeneous adsorption on the surface of EDTA- $\beta$ -CD. Therefore, only EDTA groups were considered to adsorb RE ions with relatively lower occupation ratio of adsorption sites compared to heavy metals. The adsorption capacity of RE ions following the order of La(III) < Ce(III) < Eu(III) can be explained by stability constants of lanthanides-EDTA complexes as the fact that the stability of the lanthanide EDTA complexes increase with atomic number.

In multi-component system, the competition between RE ions was observed apparently. Compared to the result of adsorption capacity in one-component system, Eu(III) showed more advantage in competing with La(III) and Ce(III). For the isotherm studies in three-component system, the extended Sips model was well fitted to the experimental data. Due to the analysis of values of adsorption capacity observed in three-component system, we got the conclusion that the affinity difference between REEs can be due to the combined effects of water structure constant and stability constant.

For the adsorption mechanism, mass transfer was not involved in adsorption mechanism in this case. Electrostatic interaction, chelation and complexation were involved in adsorption mechanism in this work based on the analysis of zeta potential and the equation of chelation and complexation. The FTIR spectra and EDS mapping after adsorption further confirmed that the RE ions were adsorbed onto the surface of EDTA- $\beta$ -CD successfully.

The application in preconcentration of EDTA- $\beta$ -CD was conducted successfully. The concentration after adsorption was much higher than the determination limits. The preconcentration method was effective for RE ions. The spent EDTA- $\beta$ -CD could be effectively regenerated by treatment with HNO<sub>3</sub> during the preconcentration study.

Overall, the novel EDTA- $\beta$ -CD showed its potential to be applied in adsorption and preconcentration of REEs from industrial wastewater or seawater.

## 9 Summary

In this master thesis, the main objective was to investigate if the novel synthesized adsorbents can adsorb REEs from aqueous phase and to test if this adsorbent could preconcentrate ultratrace REEs from seawater.

REEs are precious sources, which can be widely applied in many fields. They are dispersed and mineable REEs are scarce. Therefore, recovery and separation of REEs from aqueous phase could supplement the demand of REEs. There are many separation methods available, however, they have disadvantages. Adsorption has been studied recently and the results are quite encouraging and large amounts of adsorbents have been tested.

Adsorption can be separated into two categories based on the attraction force between adsorbent and adsorbate. There are various factors affecting adsorption, mainly pH, contact time and initial concentration. The kinetics of adsorption can be evaluated by pseudo-first-order model, pseudo-second-order model and intra-particle diffusion. There are many adsorption isotherm models, which can be applied in one-component system and multi-component systems.

Many analytical methods to quantify REEs in aqueous phase can be used. Because ICP-OES is widely used for metals, mineral and alloy, ICP was chosen as an analytical method in this work and ICP was proved to work well in this work. Many characterization methods were involved in this work. These include FTIR, elemental analysis, SEM, EDS, zeta potential measurement and TGA. In addition, COD detection was used in REEs preconcentration study.

Among all REEs, we chose La(III), Ce(III) and Eu(III) to study their adsorptive abilities. Various adsorbents have been used to adsorb La(III), Ce(III) and Eu(III) according to previous researches. Some of them were listed to compare their adsorption capacities.  $\beta$ -CD with very special structural properties is a very suitable material to complex with other material to obtain specific properties. Because of high solubility of  $\beta$ -CD, it has to be

immobilized on an insoluble support or to be cross-linked. EDTA has potential to modify  $\beta$ -CD and EDTA has been successfully used to modify chitosan or silica to remove Co(II) and Ni(II) from contaminated water based on a previous study. Therefore, we synthesized EDTA- $\beta$ -CD in a simple and green approach and used it as a potential adsorbent towards REEs.

EDTA- $\beta$ -CD polymer was prepared by polycondensation reaction of  $\beta$ -CD with EDTA. The sample preparation and batch adsorption were conducted smoothly. All the results were presented in tables and figures and interpreted. The synthesized EDTA- $\beta$ -CD were characterized via different methods. The composition of EDTA- $\beta$ -CD was calculated as the results of 64.53% for EDTA (2.21 mmol g<sup>-1</sup>) and 35.47% for  $\beta$ -CD (0.31 mmol g<sup>-1</sup>). The pH and contact time really affected adsorption capacity. The kinetic behavior fitted with pseudo-second-order model well and intra-particle diffusion also influenced on adsorption rate. The adsorption rate of studied rare earth ions follow this order: La(III)>Eu(III)>Ce(III). The maximum REEs uptake was 0.310 mmol g<sup>-1</sup> for La(III), 0.337 mmol g<sup>-1</sup> for Ce(III) and 0.353 mmol g<sup>-1</sup> for Eu(III) respectively. Langmuir model and extended Sips model were applicable for one-component system and three-component system respectively in this study.

The main conclusions are summarized as follows. The hypothesis proposed that  $\beta$ -CD do not adsorb RE ions through inclusion interaction was confirmed and only EDTA groups played the role in adsorbing RE ions with low adsorption efficiency compared to heavy metals. The stability constants of the lanthanide EDTA complexes increase with atomic number therefore affecting the adsorption capacity of RE ions. The affinity difference among REEs towards adsorbents are due to the combined effects of water structure constant and stability constant. The electrostatic interaction, chelation and complexation are involved in the adsorption mechanism in this study. The preconcentration of RE ions and regeneration of EDTA- $\beta$ -CD were proved to be successful.

To summarize, EDTA- $\beta$ -CD is an effective adsorbent to adsorb REEs, however, the adsorption capacity and regeneration efficiency still need to be improved. Further

developments on EDTA- $\beta$ -CD need to be conducted. More studies on its application in preconcentration of ultratrace REEs from seawater are still needed.

## References

- Awual R. M, Kobayashi T, Miyazaki Y, Motokawa R, Shiwaku H, Suzuki S, Okamoto Y, Yaita T. 2013. Selective lanthanide sorption and mechanism using novel hybrid Lewis base (N-methyl-N-phenyl-1,10-phenanthroline-2-carboxamide) ligand modified adsorbent. *Journal of Hazardous Materials* 252-253 page 313-320
- Awual R. M, Yaita T, Shiwaku H. 2013. Design a novel optical adsorbent for simultaneous ultra-trace cerium(III) detection, sorption and recovery. *Chemical Engineering Journal* 228 page 327-335
- Badruddoza A. Z, Tay A. S, Tan P. Y, Hidajat K, Uddin M. S. 2011. Carboxymethyl-beta-cyclodextrin conjugated magnetic nanoparticles as nano-adsorbents for removal of copper ions: synthesis and adsorption studies. *J. Hazard. Mater* 185 page 1177-86
- Cadogan I. E, Lee C. Popuri R. S, Lin H. 2014. Efficiencies of chitosan nanoparticles and crab shell particles in europium uptake from aqueous solutions through biosorption: Synthesis and characterization. *International Biodeterioration & Biodegradation* 95 page 232-240
- Chen Y, Zhu B, Wu D, Wang Q, Yang Y, Ye W, Guo J. 2012. Eu (III) adsorption using di(2-thylhexyl) phosphoric acid-immobilized magnetic GMZ bentonite. *Chemical Engineering Journal* 181-182 page 387-396
- Christmann P. 2014. A forward look into rare earth supply and demand: a role for sedimentary phosphate deposits? *Procedia Engineering* 83 page 19-26
- Crini G. 2003. Studies on adsorption of dyes on beta-cyclodextrin polymer. *Bioresour. Technol.* 90 page 193-8
- Das D, Varshini C S. J, Das N. 2014. Recovery of lanthanum(III) from aqueous solution using biosorbents of plant and animal origin: Batch and column studies. *Minerals*

Engineering 69 page 40-56

Durand S, Dognon J, Guilbaud P, Rabbea C, Wipff G. 2000. Lanthanide and alkaline-earth complexes of EDTA in water: a molecular dynamics study of structures and binding selectivities. *J. Chem. Soc.* 2 page 705-714

Esser K. Bradley, Volpe A, Kenneally M. Jacqueline, Smith K. David. 1994. Preconcentration and Purification of Rare Earth Elements in Natural Waters Using Silica-Immobilized 8-Hydroxyquinoline and a Supported Organophosphorus Extractant. *Anal. Chem.* 66 (10) page 1736–1742

Fuhrer R, Herrmann I. K, Athanassiou E. K, Grass R. N, Stark W. J. 2011. Immobilized beta-cyclodextrin on surface-modified carbon-coated cobalt nanomagnets: reversible organic contaminant adsorption and enrichment from water. *Langmuir* 27 page 1924-9

Gasser M.S & Aly M.I. 2013. Separation and recovery of rare earth elements from spent nickel - metal-hydride batteries using synthetic adsorbent. *International Journal of Mineral Processing* 121 page 31-38

Gidwani B, Vyas A. 2014. Synthesis, characterization and application of epichlorohydrin-beta-cyclodextrin polymer. *Colloids Surf. B Biointerfaces* 114 page 130-7

Granados-Correa F, Jiménez-Reyes M. 2011. Combustion Synthesis of BaCO<sub>3</sub> and its Application for Eu(III) Adsorption from Aqueous Solution. *Separation Science and Technology* Volume 46 pages 2360-2366

Granados-Correa F, Vilchis-Granados J, Jiménez-Reyes M., Quiroz-Granados L. A. 2012. Adsorption Behaviour of La(III) and Eu(III) Ions from Aqueous Solutions by Hydroxyapatite: Kinetic, Isotherm, and Thermodynamic Studies. *Journal of Chemistry*. Volume 2013, 9 pages

Grebneva O.N., Kuz'min N.M., Tsysin G.I., Zolotov Yu.A. 1996. On-line-sorption

preconcentration and inductively coupled plasma atomic emission spectrometry determination of rare earth elements. *Spectrochimica Acta Part B: Atomic Spectroscopy* 51 pages 1417–1423

Gordon B. Haxel, James B. Hedrick, Greta J. Orris. 2002. Rare Earth Elements—Critical Resources for High Technology. U.S. Geological Survey page 087-02

Han C, Zhang L, Li H. 2009. Highly selective and sensitive colorimetric probes for Yb<sup>3+</sup> ions based on supramolecular aggregates assembled from  $\beta$ -cyclodextrin-4, 4'-dipyridine inclusion complex modified silver nanoparticles. The Royal Society of Chemistry.

Heinonen K. A. 2012. Adsorption of hydrogen sulfide using modified cellulose nano/micro crystals. Master's Thesis. Lappeenranta University of Technology. Faculty of Technology.

Hirakawa B, Epichlorohydrin. 2014. In *Encyclopedia of Toxicology (Third Edition)*, Wexler, P., Ed. Academic Press: Oxford page 431-432

Hokkanen S, Repo E, Sillanpää M. 2013. Removal of heavy metals from aqueous solutions by succinic anhydride modified mercerized nanocellulose. *Chem.Eng.J.* 223 page 40-47

ICES International Council for the Exploration of the Sea (ICES), Oceanographic Database. CTD and Bottle Data (2015) <http://ocean.ices.dk/HydChem/HydChem.aspx?plot=yes> (updated 2015.04.09)

Ito K, Masukawa F, Mao Q, Hirokawa T. 1998. Inductively coupled plasma-atomic emission spectral fitting analysis of rare-earth elements in ion-adsorption type ores. *Analytica Chimica Acta* 362 page 241-245

Kawabe I. 2014. Stability constants of lanthanide(III)-EDTA complex formation and Gd-break with tetrad effect in their series variation [online document]. [Accessed 12 June 2014] Available at <http://hdl.handle.net/2237/20251>

Kawano S, Kida T, Miyawaki K, Noguchi Y, Kato E, Nakano T, Akashi M. 2014. Cyclodextrin Polymers as Highly Effective Adsorbents for Removal and Recovery of Polychlorobiphenyl (PCB) Contaminants in Insulating Oil. *Environ. Sci. Technol.* 48, 8094-8100

Keith Veronese. *Rare: The High-Stakes Race to Satisfy Our Need for the Scarcest Metals on Earth*. ISBN: 978-1-61614-972-7. 270 pages

Konkena B, Vasudevan S. 2012. Covalently linked, water-dispersible, cyclodextrin: reduced-graphene oxide sheets. *Langmuir* 28 page 12432-7

Ladavos K. A, Katsoulidis P. A, Iosifidis A, Triantafyllidis S. K, Pinnavaia J. T, Pomonis J. P. 2012. The BET equation, the inflection points of  $N_2$  adsorption isotherms and the estimation of specific surface area of porous solids. *Microporous and Mesoporous Materials* 151 page 126-133

Li S, Hu B, Jiang Z, Liang P, Li X, Xia L. 2004. Selective separation of  $La^{3+}$  and lanthanum organic complexes with nanometer-sized titanium dioxide and their detection by using fluorination-assisted electrothermal vaporization ICP-AES with in-situ matrix removal. *Environ Sci Technol* 38 (7) page 2248-51

Liang P, Liu Y, Guo L. 2005. Determination of trace rare earth elements by inductively coupled plasma atomic emission spectrometry after preconcentration with multiwalled carbon nanotubes. *Spectrochimica Acta Part B: Atomic Spectroscopy* Volume 60 pages 125–129

Liang P, Hu B, Jiang Z, Qin Y, Peng T. 2001. Nanometer-sized titanium dioxide micro-column on-line preconcentration of La, Y, Yb, Eu, Dy and their determination by inductively coupled plasma atomic emission spectrometry. *J. Anal. At. Spectrom.* 16 page 863-866

Liu H, Cai, X, Wang Y, Chen J. 2011. Adsorption mechanism-based screening of cyclodextrin polymers for adsorption and separation of pesticides from water. *Water Res.*

45 page 3499-511

Li Y. F, Ha Y. M, Guo Q, Li Q. P. 2015. Synthesis of two beta-cyclodextrin derivatives containing a vinyl group. *Carbohydr. Res.* 404 page 55-62

Luo S, Xu X, Zhou G, Liu C, Tang Y, Liu Y. 2014. Amino siloxane oligomer-linked graphene oxide as an efficient adsorbent for removal of Pb(II) from wastewater. *Journal of Hazardous Materials* Volume 274 pages 145–155

Lou Z, Wan L, Guo C, Zhang S, Shan W, Xiong Y. 2015. Quasi-complete Separation Re(VII) from Mo(VI) onto Magnetic Modified Cross-Linked Chitosan Crab Shells Gel by Using Kinetics Methods. *Ind. Eng. Chem. Res.* 54 (4) page 1333–1341

Mahmoud R. M, Sharaf El-deen E. G, Soliman A. M. 2014. Surfactant-impregnated activated carbon for enhanced adsorptive removal of Ce(IV) radionuclides from aqueous solutions. *Annals of Nuclear Energy* 72 page 134-144

Medronho B, Andrade R, Vivod V, Ostlund A, Miguel M. G, Lindman B, Voncina B, Valente A. J. 2013. Cyclodextrin-grafted cellulose: physico-chemical characterization. *Carbohydr. Polym.* 93 page 324-30

Michels J. J, Huskens J, Reinhoudt N. D. 2002. Noncovalent Binding of Sensitizers for Lanthanide(III) Luminescence in an EDTA-bis( $\beta$ -cyclodextrin) Ligand. *J. Am. Chem. Soc.* 124 (9) page 2056–2064

Moldoveanu A. G, Papangelakis G. V. 2012. Recovery of rare earth elements adsorbed on clay minerals: I. Desorption mechanism. *Hydrometallurgy* 117 - 118 page 71-78

Murty D. S. R, Chakrapani G. 1996. Preconcentration of rare earth elements on activated carbon and its application to groundwater and sea-water analysis. *J. Anal. At. Spectrom.* 11 page 815-820

Nash L. K, Brigham D, Sheheea C. T, Martina A. 2012. The kinetics of lanthanide complexation by EDTA and DTPA in lactate media. *Dalton Trans.*41 page 14547-14556

Ngomsik F. A, Bee A, Talbot D, Cote G. 2012. Magnetic solid - liquid extraction of Eu(III), La(III), Ni(II) and Co(II) with maghemite nanoparticles. *Separation and Purification Technology* 86 page 1-8

Pasinli T, Erođlu E. A, Shahwan T. 2005. Preconcentration and atomic spectrometric determination of rare earth elements (REEs) in natural water samples by inductively coupled plasma atomic emission spectrometry. *Analytica Chimica Acta* 547 page 42-49

Pearson G. R. 1963. Hard and Soft Acids and Bases. *J. Am. Chem. Soc.*85 (22) page 3533–3539

Ponou J, Wang P. L, Dodbiba G, Okaya K, Fujita T, Mitsunashi K, Atarashi T, Satoh G, Noda M. 2014. Recovery of rare earth elements from aqueous solution obtained from Vietnamese clay minerals using dried and carbonized parachlorella. *Journal of Environmental Chemical Engineering* 2 page 1070-1081

Rahman M. M, Khan B. S, Marwani M. H, Asiri M. A. 2014. SnO<sub>2</sub> - TiO<sub>2</sub> nanocomposites as new adsorbent for efficient removal of La(III) ions from aqueous solutions. *Journal of the Taiwan Institute of Chemical Engineers* 45 page 1964-1974

Repo E, Warchol J. K, Kurniawan T. A, Sillanpää M. E. T. 2010. Adsorption of Co(II) and Ni(II) by EDTA- and/or DTPA-modified chitosan: Kinetic and equilibrium modeling. *Chem. Eng. J.* 161 page 73-82

Schofield W. C. E, Bain C. D, Badyal J. P. S. 2012. Cyclodextrin-Functionalized Hierarchical Porous Architectures for High-Throughput Capture and Release of Organic Pollutants from Wastewater. *Chem. Mater.* 24 page 1645-1653

Sert Ş, Kütahyalı C, İnan S, Talip Z, Çetinkaya B, Eral M. 2008. Biosorption of lanthanum

and cerium from aqueous solutions by *Platanus orientalis* leaf powder. *Hydrometallurgy* Volume 90 pages 13–18

Sobocinski J, Laure W, Taha M, Courcot E, Chai F, Simon N, Addad A, Martel B, Haulon S, Woisel P, Blanchemain N, Lyskawa J. 2014. Mussel inspired coating of a biocompatible cyclodextrin based polymer onto CoCr vascular stents. *ACS Appl. Mater. Inter.* 6 page 3575-86

Stephen B. C, James B. H. Rare earth elements. *Industrial Minerals and Rocks* [online document]. [Accessed 27 October 2014]. Available at <http://www.segemar.gov.ar/bibliotecaintemin/LIBROSDIGITALES/Industrialminerals%26rocks7ed/pdf/papers/058.pdf>

Tadjarodi A, Jalalat V, Dorabei Z. R. 2014. Adsorption of La (III) in aqueous systems by N-(2-hydroxyethyl) salicylaldimine-functionalized mesoporous silica. *Materials Research Bulletin* 61 page 113-119

Tan X, Fan Q, Wang X, Grambow B. 2009. Eu(III) Sorption to TiO<sub>2</sub> (Anatase and Rutile): Batch, XPS, and EXAFS Studies. *Environ. Sci. Technol.* 43 (9) page 3115–3121

Vijayaraghavan K, Balasubramanian R. 2010. Single and binary biosorption of cerium and europium onto crab shell particles. *Chemical Engineering Journal*

Vijayaraghavana K, Sathishkumara M, Balasubramanian R. 2011. Interaction of rare earth elements with a brown marine alga in multi-component solutions. *Desalination* Volume 265 pages 54–59

Wen B, Shan X, Xu S. 1999. Preconcentration of ultratrace rare earth elements in seawater with 8-hydroxyquinoline immobilized polyacrylonitrile hollow fiber membrane for determination by inductively coupled plasma mass spectrometry. *Analyst* 124 page 621-626

Wilson L. D, Pratt D. Y, Kozinski J. A. 2013. Preparation and sorption studies of beta-

cyclodextrin-chitosan-glutaraldehyde terpolymers. *J. Colloid Interface Sci.* 393 page 271-7

Wolf E. R. 2005. Introduction to ICP-MS [online document]. [Accessed March 2005]. Available at <http://crustal.usgs.gov/laboratories/icpms/intro.html>

Wu D, Zhu C, Chen Y, Zhu B, Yang Y, Wang Q, Ye W. 2012. Preparation, characterization and adsorptive study of rare earth ions using magnetic GMZ bentonite. *Applied Clay Science* 62-63 page 87-93

Yao C. 2010. Adsorption and desorption properties of D151 resin for Ce(III). *JOURNAL OF RARE EARTHS* 28 page 183

Yu O. Y, Chung J. W, Kwak S. Y. 2008. Reduced migration from flexible poly(vinyl chloride) of a plasticizer containing beta-cyclodextrin derivative. *Environ. Sci. Technol.* 42 page 7522-7

Zeiger E, Gollapudi B, Spencer P. 2005. Genetic toxicity and carcinogenicity studies of glutaraldehyde—a review. *Mutat. Res.-Rev. Mutat* 589 page 136-151

Zhang L, Ding S. D, Yang T, Zheng G.C. 2009. Adsorption behavior of rare earth elements using polyethyleneglycol (phosphomolybdate and tungstate) heteropolyacid sorbents in nitric solution. *Hydrometallurgy* 99 page 109-114

Zhao F, Repo E, Sillanpää M, Meng Y, Yin D, Tang W. Z. 2015. Green Synthesis of Magnetic EDTA- and/or DTPA-Cross-Linked Chitosan Adsorbents for Highly Efficient Removal of Metals. *Ind. Eng. Chem. Res.* 54 page 1271-1281

Zhao F, Repo E, Yin D, Sillanpää E.T. M. 2013. Adsorption of Cd(II) and Pb(II) by a novel EGTA-modified chitosan material: Kinetics and isotherms. *Journal of Colloid and Interface Science* 409 page 174-182

Zhao F, Tang Z. Walter, Zhao D, Meng Y, Yin D, Sillanpää E.T. M. 2014. Adsorption kinetics,

isotherms and mechanisms of Cd(II), Pb(II), Co(II) and Ni(II) by a modified magnetic polyacrylamide microcomposite adsorbent. *Journal of Water Process Engineering* 4 page 47-57

Zhao D, Zhao L, Zhu C, Tian Z, Shen X. 2009. Synthesis and properties of water-insoluble  $\beta$ -cyclodextrin polymer crosslinked by citric acid with PEG-400 as modifier. *Carbohydr. Polym.* 78 page 125-130

Zhu Y, Zheng Y, Wang A. 2015. A simple approach to fabricate granular adsorbent for adsorption of rare elements. *International Journal of Biological Macromolecules* 72 page 410-420